Eur. Phys. J. C 52, 857–874 (2007)
DOI 10.1140/epjc/s10052-007-0436-y

THE EUROPEAN PHYSICAL JOURNAL C

Regular Article – Experimental Physics

Production of V^0 pairs in the hyperon experiment WA89

The WA89 Collaboration

M.I. Adamovich[1,a], Yu.A. Alexandrov[1,b], S.P. Baranov[1,b], D. Barberis[2], M. Beck[3], C. Bérat[4], W. Beusch[5], M. Boss[6], S. Brons[3,10], W. Brückner[3], M. Buénerd[4], C. Busch[6], C. Büscher[3], F. Charignon[4], J. Chauvin[4], E.A. Chudakov[6,11], U. Dersch[3], F. Dropmann[3], J. Engelfried[6,12], F. Faller[6,13], A. Fournier[4], S.G. Gerassimov[3,1,14], M. Godbersen[3], P. Grafström[5], T. Haller[3], M. Heidrich[3], E. Hubbard[3], R.B. Hurst[2], K. Königsmann[3,15], I. Konorov[3,1,14], S. Kovalenko[7], N. Keller[6], K. Martens[6,16], P. Martin[4], S. Masciocchi[3,17], R. Michaels[3,11], U. Müller[8], H. Neeb[3], D. Newbold[9], C. Newsom[18], S. Paul[3,14], J. Pochodzalla[3,6], I. Potashnikova[3,7,c], B. Povh[3], Z. Ren[3], M. Rey-Campagnolle[4,19], G. Rosner[8,20], L. Rossi[2], H. Rudolph[8], C. Scheel[21], L. Schmitt[8,17], H.-W. Siebert[6,8], A. Simon[7,15], V. Smith[9], O. Thilmann[7], A. Trombini[3], E. Vesin[4], B. Volkemer[8], K. Vorwalter[3], T. Walcher[8], G. Wälder[7], R. Werding[3], E. Wittmann[3], M.V. Zavertyaev[1,b,c,d]

[1] Moscow Lebedev Physics Institute, Leninsky pr. 53, 117924, Moscow, Russia
[2] Dipartimento di Fisica and I.N.F.N, Sezione di Genova, 16146 Genova, Italy
[3] Max-Planck-Institut für Kernphysik Heidelberg, 69029 Heidelberg, Germany
[4] Institut des Sciences Nucléaires, Université de Grenoble, 38026 Grenoble Cedex, France
[5] CERN, 1211 Genève 23, Switzerland
[6] Physikalisches Institut, Universität Heidelberg, 69120 Heidelberg, Germany[e]
[7] Departamento de Física y Centro de Estudios Subatómicos, Universidad Técnica Federico Santa María, Casilla 110-V, Valparaíso, Chile
[8] Institut für Kernphysik, Universität Mainz, 55099 Mainz, Germany[e]
[9] University of Bristol, Bristol BS8 1TL, UK
[10] Now at TRIUMF, Vancouver, B.C., Canada V6T 2A3
[11] Now at Thomas Jefferson Lab, Newport News, VA 23606, USA
[12] Now at Instituto de Fisica, Universidad Autonoma de San Luis Potosi, S.L.P. 78240 Mexico
[13] Now at Fraunhofer Institut für Solar Energiesysteme, 79100 Freiburg, Germany
[14] Now at Physik Department E18, Technische Universitaät München, 85747 Garching, Germany
[15] Now at Fakultät für Physik, Universität Freiburg, Germany
[16] Now at Department of Physics, University of Utah, Salt Lake City, Utah, USA
[17] Now at Gesellschaft für Schwerionenforschung, 64291 Darmstadt, Germany
[18] University of Iowa, Iowa City, Iowa 52242, USA
[19] Permanent address: CERN, 1211 Genève 23, Switzerland
[20] Now at Department of Physics and Astronomy, University of Glasgow, Glasgow G12 8QQ, UK
[21] NIKHEF, 1009 D8 Amsterdam, The Netherlands

Received: 9 September 2007 / Revised version: 25 September 2007 /
Published online: 17 October 2007 –

Abstract. We present a comprehensive study of the inclusive production of V^0V^0 pairs ($V^0 = \Lambda, \overline{\Lambda}$ or K_S) by Σ^- and π^- of 340 GeV/c momentum and neutrons of 260 GeV/c mean momentum in copper and carbon targets. In particular, the dependence of the x_F spectra on the combination of beam-particle and produced V^0V^0 pair is investigated and compared to predictions obtained from PYTHIA and QSGM calculations. The data and these predictions differ in many details, the agreement can at best be termed as qualitative. A signal from decays of the tensor meson $f_2'(1525)$ was observed in the K_S K_S mass distribution and inclusive production cross sections were measured. No signal was found from the double-strange H-dibaryon decaying to $\Lambda\Lambda$.

[a] Deceased

[b] Supported by Deutsche Forschungsgemeinschaft, contract number 436 RUS 113/465/0-2(R), and Russian Foundation for Basic Research under contract number RFFI 00-02-04018.

[c] Supported in part by Fondecyt (Chile) grants 1050519 and 7050178.

[d] e-mail: Mikhail.Zavertiaev@mpi-hd.mpg.de

[e] Supported by the Bundesministerium für Bildung, Wissenschaft, Forschung und Technologie, Germany, under contract numbers 05 5HD15I, 06 HD524I and 06 MZ5265.

1 Introduction

In a previous publication [1], we have reported a measurement of inclusive production cross sections of Λ, $\overline{\Lambda}$ and K_S produced by Σ^- and π^- of 340 GeV/c momentum and neutrons of 260 GeV/c average momentum incident on nuclear targets. We have also published a study of momentum spectra and correlations in $\Lambda\overline{\Lambda}$ pairs produced by Σ^- and neutrons [2].

A large number of Λ, $\overline{\Lambda}$ and K_S (jointly called V^0 in the following) were observed in our experiment, for instance $2\times10^6\Lambda$, $1.5\times10^5\overline{\Lambda}$ and $2\times10^6 K_S$ produced by Σ^- in the data collected in 1993. This gave us an opportunity to study inclusive V^0V^0 pair production with samples of up to 12000 observed pairs per channel. These statistics are sufficient to study correlations between the daughter momenta, which can provide new information about hadron production processes, in particular the role of strange quarks in these processes and the leading particle effect.

We have also searched for resonance signals in the V^0V^0 mass spectra, in particular the possibly existing H dibaryon in the $\Lambda\Lambda$ sample.

V^0V^0 pairs have been studied in two previous experiments: In an experiment at FERMILAB using the 15-ft. bubble chamber placed in a π^- beam, about 100 pairs each of K_SK_S and ΛK_S were found [3]. At CERN, the WA97 collaboration collected 2000 K_SK_S pairs and 1200$\Lambda\Lambda$ pairs produced centrally in Pb–Pb collisions at 158 GeV/A. These were used to study Hanbury–Brown–Twiss momentum correlations and to search for the H-dibaryon, respectively [4].

2 Hyperon beam and experimental apparatus

The hyperon beam was derived from an external proton beam of the CERN-SPS, hitting a hyperon production target placed 16 m upstream of the experimental target. Negative secondaries with a mean momentum of 340 GeV/c and a momentum spread $\sigma(p)/p\approx9\%$ were selected in a magnetic channel. At the experimental target, the beam consisted of π^-, Σ^-, K^- and Ξ^- in the ratio 2.3 : 1 : 0.025 : 0.008. A transition radiation detector (TRD) made up of 10 MWPCs interleaved with foam radiators allowed to select Σ^- or π^- at the trigger level [5]. Typically, about $1.8\times10^5\Sigma^-$ and $4.5\times10^5\pi^-$ were delivered to the target during one SPS-spill, which had an effective length of about 1.5 s. More details can be found in [6].

Σ^- decays upstream of the target were the source of neutrons used in our measurement. The momenta of these neutrons were defined as the difference between the average Σ^- momentum and the momentum of the decay π^- measured in the spectrometer. The neutron spectrum had an average momentum of 260 GeV/c and a momentum spread $\sigma(p)/p=15\%$.

The experimental target was situated 3.6 m downstream of the exit of the last beam magnet. It consisted of one copper and three carbon blocks arranged in a row along the beam, with thicknesses corresponding to $0.026\lambda_I$ and three times $0.0083\lambda_I$, respectively. Microstrip detectors upstream and downstream of the target allowed to measure the tracks of the incoming beam particles and of the charged particles produced in the target blocks.

The target was positioned 14 m upstream of the center of the Omega spectrometer magnet [7] so that a field-free decay region of 10 m length was provided for hyperon and K_S decays. Tracks of charged particles were measured inside the magnet and in the field-free regions upstream and downstream by MWPCs and driftchambers, with a total of 130 planes. The Omega magnet provided a field integral of 7.5 Tm, and the momentum resolution achieved was $\sigma(p)/p^2\approx10^{-4}$ (GeV/c)$^{-1}$.

Downstream of the spectrometer, a ring-imaging Cherenkov detector, an electromagnetic calorimeter and a hadron calorimeter were placed, which were not used in this analysis.

The main trigger selected about 25% of all interactions, using multiplicities measured in microstrip counters upstream and downstream of the target and in scintillator hodoscopes and MWPCs behind the Omega magnet. Correlations between hits in different detectors were used in the trigger to increase the fraction of events with high-momentum particles, thus reducing background from low-momentum pions in the beam. Beam Σ^- were identified online by the TRD. A sample of pion interactions was obtained by inverting the online TRD decision for a fraction of the runs. In addition, a reduced sample of beam triggers was recorded for trigger calibration purposes. The results presented in this article are based on 100 million Σ^- interactions, 7 million neutron interactions and 6 million π^- interactions recorded in the year 1993. This data set is identical to the one used for the previous studies published in [1, 2]. The results for $\Lambda\overline{\Lambda}$ pairs presented here are identical to those published in [2].

3 Event selection

Each event had to have one reconstructed beamtrack and an interaction vertex containing at least two outgoing charged tracks reconstructed in the microstrip counters downstream of the target. The reconstructed vertex position had to be within a target block where in each coordinate an additional margin of 3σ was allowed.

For Σ^- and π^- beam interactions, the transverse distance between the beam track and the reconstructed vertex position was required to be less than 6σ ($\sigma\approx25\ \mu$m). In the case of neutron interactions the beam track was assumed to come from a Σ^- decay upstream of the target, and it therefore had to miss the reconstructed interaction point by a distance of at least 6σ. This π^- candidate track had to be connected to a negative particle track in the spectrometer with a momentum smaller than 140 GeV/c corresponding to the $\Sigma^-\to n\pi^-$ decay kinematics at $<p>\approx340$ GeV/c. are identical to those published in [2].

V^0 candidates then were selected from all pairs of positive and negative tracks which formed a vertex in the decay zone between the microstrip detectors downstream of the target and the Omega magnet. The distance between the two tracks at the decay point had to be smaller than 3 mm. The V^0 trajectory reconstructed from the decay particles had to have a transverse distance to the interaction vertex of less than 12 mm. In Fig. 1 we show the spectra of the masses reconstructed assuming $\Lambda \to p\pi^-$, $\overline{\Lambda} \to \pi^+\overline{p}$ or $K_S \to \pi + \pi^-$ decays. The observed mass peaks are centered at 1115.7 ± 0.1, 1115.6 ± 0.4 and $496.6 \pm 0.4\,\mathrm{MeV}/c^2$, in good agreement with the Λ, $\overline{\Lambda}$ and K^0 masses respectively. The mass resolution is about $\sigma = 2\,\mathrm{MeV}/c^2$ for Λ and $\overline{\Lambda}$ and $\sigma = 4.5\,\mathrm{MeV}/c^2$ for K_S. V^0 candidates with reconstructed masses within $\pm 15\,\mathrm{MeV}/c^2$ of the peak center and with a total momentum below $260\,\mathrm{GeV}/c$ were retained for further analysis. In addition, background from $\gamma \to e^+e^-$ conversion was suppressed on the basis of the Armenteros plot (Fig. 2) requiring that the transverse momenta of the decay tracks with respect to the V^0 direction had to be greater than $15\,\mathrm{MeV}/c$.

V^0V^0 pair candidates were taken from this sample, with the additional requirement the two V^0 have no decay track in common and that both V^0 have $x_\mathrm{F} > 0$.

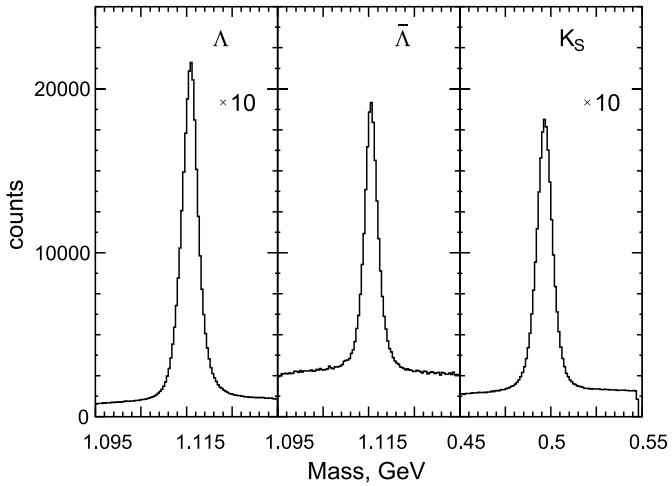

Fig. 1. The invariant mass distribution of V^0 produced in Σ^- beam

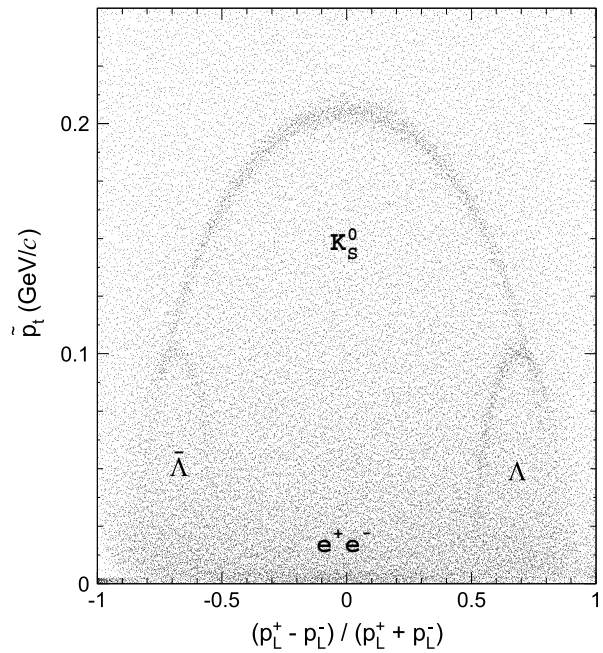

Fig. 2. Armenteros–Podolanski plot of V^0 candidates. e^+e^- pairs were cut at $p_\mathrm{t} = 0.015\,\mathrm{GeV}/c$. $p_\mathrm{L}^\pm$ and p_t are the laboratory longitudinal and transverse momenta of the positive and negative decay particles with respect to the V^0 direction

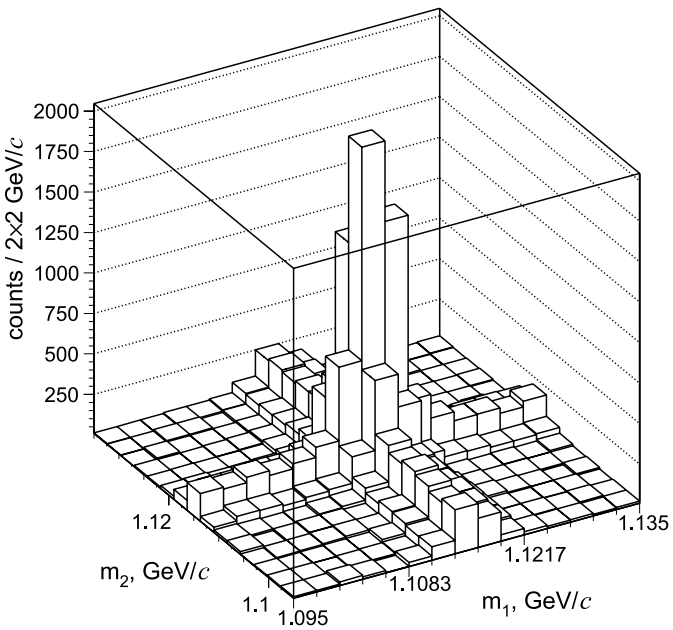

Fig. 3. Two-dimensional mass distribution of $\Lambda\Lambda$ candidates

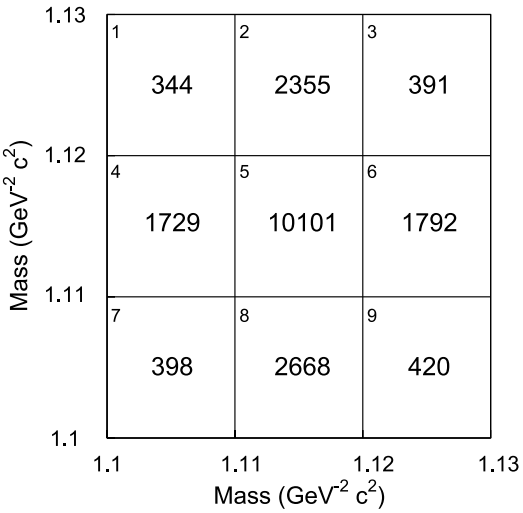

Fig. 4. 3 by 3 bin plot for the determination of the number of real $\Lambda\Lambda$ pairs

Table 1. V^0V^0 production cross sections in copper and carbon in mb

Beam	Neutrons		π^-		Σ^-	
Target	Copper	Carbon	Copper	Carbon	Copper	Carbon
$\Lambda\Lambda$	1.7 ± 0.1	0.44 ± 0.03	1.0 ± 0.1	0.27 ± 0.02	5.5 ± 0.1	1.57 ± 0.02
$\Lambda\overline{\Lambda}$	3.7 ± 0.2	1.0 ± 0.1	6.8 ± 0.2	1.9 ± 0.1	7.4 ± 0.1	2.38 ± 0.02
ΛK_S	6.8 ± 0.2	1.9 ± 0.1	4.4 ± 0.1	1.19 ± 0.04	12.8 ± 0.1	4.01 ± 0.02
$\overline{\Lambda\Lambda}$	0.04 ± 0.02	0.01 ± 0.01	0.13 ± 0.03	0.05 ± 0.01	0.11 ± 0.01	0.03 ± 0.01
$\overline{\Lambda} K_S$	0.49 ± 0.05	0.26 ± 0.03	2.1 ± 0.1	0.6 ± 0.03	1.63 ± 0.03	0.51 ± 0.01
$K_S K_S$	1.6 ± 0.1	0.46 ± 0.03	2.9 ± 0.1	0.82 ± 0.03	2.92 ± 0.03	0.88 ± 0.01

Table 2. The signals of the V^0 pairs, observed in the experiment

Beam	Neutrons		π^-		Σ^-	
Target	Copper	Carbon	Copper	Carbon	Copper	Carbon
$\Lambda\Lambda$	135 ± 15	123 ± 14	127 ± 16	99 ± 15	6217 ± 111	5516 ± 96
$\Lambda\overline{\Lambda}$	270 ± 19	236 ± 13	853 ± 32	731 ± 30	7827 ± 104	7707 ± 103
ΛK_S	862 ± 33	777 ± 31	867 ± 35	734 ± 30	24819 ± 181	23835 ± 177
$\overline{\Lambda\Lambda}$	5 ± 3	4 ± 2	15 ± 5	16 ± 5	74 ± 14	58 ± 13
$\overline{\Lambda} K_S$	39 ± 11	56 ± 10	300 ± 23	236 ± 22	1804 ± 62	1666 ± 60
$K_S K_S$	232 ± 19	189 ± 17	797 ± 32	700 ± 31	6617 ± 101	6368 ± 101

4 V^0V^0 production cross sections

4.1 Analysis procedure

In order to estimate the true number of V^0V^0 pairs above the background of $h^+h^-h^+h^-$ and $V^0h^+h^-$ combinations

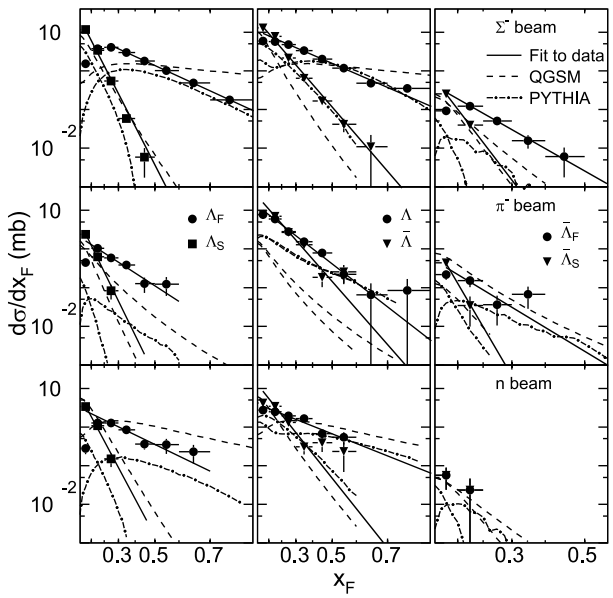

Fig. 5. Differential cross sections of inclusive $\Lambda\Lambda$, $\Lambda\overline{\Lambda}$ and $\overline{\Lambda\Lambda}$ pair production by Σ^-, π^- and neutrons in carbon, as a function of x_F. Only statistical errors are shown. *Full lines*: fits to the data (see Sect. 4.2), *dotted* and *dot-dashed lines*: Monte Carlo calculations (see Sect. 6.2). The particle subscripts F and S refer to fast and slow

(h means proton, anti-proton or pion depending on the V^0 type) we used a two-dimensional plot of the invariant masses $M(h^+h^-)_1$ and $M(h^+h^-)_2$. In Fig. 3 a Lego plot is shown for $\Lambda\Lambda$ mass combinations produced by Σ^-.

Figure 4 shows the same sample in a scatter plot of 10 MeV-by-10 MeV bins where Δm is the difference between the reconstructed mass and the peak center mass, thus the central square is centered on the V^0 mass for each axis. The background due to $h^+h^-h^+h^-$ production was estimated with the four outside corners of the plot. First the mean content of these four squares was subtracted from every square. Then we subtracted half the content of the $V^0h^+h^-$ and $h^+h^-V^0$ side bands from the central mass bin to obtain the genuine V^0V^0 signal. For the plot shown, the result is $N_{V^0V^0} = 6217 \pm 111$. The signal statistics after background subtraction are shown in Table 2 for each V^0V^0 and beam combination.

The differential cross section as a function of the Feynman variable x_F and the squared transverse momentum p_t^2 [1] was calculated by the following formula:

$$\sigma\left(x_{F,1}, p^2_{t,1}, x_{F,2}, p^2_{t,2}\right) = \frac{1.}{BR\left(V^0_1\right) \cdot BR\left(V^0_2\right)} \times \frac{N_{V^0V^0}}{\varepsilon\left(i_1, x_{F,1}, p^2_{t,1}\right) \varepsilon\left(i_2, x_{F,2}, p^2_{t,2}\right) N_b \rho l N_A / M} . \quad (1)$$

Here $N_{V^0V^0}$ is the number of observed V^0V^0 in the particular region of the corresponding kinematic variables

[1] Feynman-x is calculated here as $x_F = 2p^*_L/\sqrt{s}$, where p^*_L is the momentum component in beam direction in the (beam particle, target nucleon) rest system. p_t is the momentum component transverse to the beam and $\sqrt{s}$ is the invariant (beam particle, target nucleon) mass.

Table 3. The fit parameter values of the differential cross section approximation in form of $\mathrm{d}^2\sigma/\mathrm{d}p_\mathrm{t}^2\,\mathrm{d}x_\mathrm{F} = C(1-x_\mathrm{F})^n \exp(-Bp_\mathrm{t}^2)$ with their fit errors (see text), copper target

Beam		Neutrons		π^-		Σ^-	
Target		n	B	n	B	n	B
$\Lambda\Lambda$	ΛF	4.6 ± 0.9	2.0 ± 0.3	4.6 ± 0.5	2.1 ± 0.3	3.4 ± 0.2	2.06 ± 0.04
	ΛS	13.6 ± 1.2	1.9 ± 0.2	14.6 ± 1.2	2.6 ± 0.2	13.2 ± 0.2	2.21 ± 0.04
$\Lambda\overline{\Lambda}$	Λ	3.8 ± 0.4	2.3 ± 0.2	5.5 ± 0.3	2.3 ± 0.1	3.3 ± 0.1	2.26 ± 0.03
	$\overline{\Lambda}$	9.9 ± 1.0	2.8 ± 0.3	6.4 ± 0.4	2.4 ± 0.1	7.5 ± 0.1	2.41 ± 0.03
ΛK_S	Λ	3.6 ± 0.5	2.2 ± 0.1	5.4 ± 0.2	2.4 ± 0.1	3.5 ± 0.1	2.22 ± 0.02
	K_S	6.0 ± 0.7	2.3 ± 0.1	4.9 ± 0.3	2.0 ± 0.1	6.1 ± 0.1	1.89 ± 0.02
$\overline{\Lambda\Lambda}$	$\overline{\Lambda}F$	–	–	5.4 ± 2.5	1.7 ± 0.6	11.0 ± 2.0	2.5 ± 0.2
	$\overline{\Lambda}S$	–	–	10.0 ± 3.0	1.9 ± 0.8	19.0 ± 2.0	2.4 ± 0.2
$\overline{\Lambda}K_\mathrm{S}$	$\overline{\Lambda}$	10.0 ± 2.0	2.7 ± 0.3	7.8 ± 0.8	2.5 ± 0.2	9.7 ± 0.4	2.4 ± 0.1
	K_S	4.0 ± 1.0	1.8 ± 0.3	5.0 ± 0.6	2.0 ± 0.1	3.9 ± 0.2	1.9 ± 0.1
$K_\mathrm{S}K_\mathrm{S}$	$K_\mathrm{S}F$	8.0 ± 2.0	1.9 ± 0.2	5.2 ± 0.4	1.9 ± 0.1	4.7 ± 0.2	1.92 ± 0.05
	$K_\mathrm{S}S$	5.0 ± 2.0	1.9 ± 0.2	11.0 ± 1.0	2.4 ± 0.1	12.2 ± 0.4	1.96 ± 0.03

Table 4. The fit parameter values of the differential cross section approximation in form of $\mathrm{d}^2\sigma/\mathrm{d}p_\mathrm{t}^2\,\mathrm{d}x_\mathrm{F} = C(1-x_\mathrm{F})^n \exp(-Bp_\mathrm{t}^2)$ with their fit errors (see text), carbon target. The subscripts L and N indicate the leading and non-leading particles, respectively

Beam		Neutrons		π^-		Σ^-	
		n	B	n	B	n	B
$\Lambda\Lambda$	Λ_L	3.1 ± 0.7	1.8 ± 0.3	4.2 ± 0.6	2.2 ± 0.4	3.0 ± 0.2	2.26 ± 0.04
	Λ_N	12.0 ± 1.0	3.4 ± 0.4	13.0 ± 1.0	2.6 ± 0.2	12.6 ± 0.2	2.34 ± 0.04
$\Lambda\overline{\Lambda}$	Λ	2.6 ± 0.4	2.5 ± 0.2	4.9 ± 0.3	2.5 ± 0.1	2.8 ± 0.1	2.42 ± 0.03
	$\overline{\Lambda}$	8.0 ± 1.0	2.8 ± 0.2	7.3 ± 0.5	2.5 ± 0.1	7.5 ± 0.1	2.56 ± 0.03
ΛK_S	$\overline{\Lambda}$	4.0 ± 0.4	2.4 ± 0.1	4.7 ± 0.2	2.6 ± 0.1	3.0 ± 0.1	2.36 ± 0.02
	K_S	5.2 ± 0.6	2.5 ± 0.1	5.5 ± 0.4	2.0 ± 0.1	5.5 ± 0.2	2.01 ± 0.02
$\overline{\Lambda\Lambda}$	$\overline{\Lambda}_\mathrm{L}$	–	–	8.0 ± 4.0	2.1 ± 0.6	7.0 ± 1.0	2.6 ± 0.2
	$\overline{\Lambda}_\mathrm{N}$	–	–	20.0 ± 6.0	3.6 ± 0.9	17.0 ± 2.0	3.5 ± 0.4
$\overline{\Lambda}K_\mathrm{S}$	$\overline{\Lambda}$	14.0 ± 3.0	2.6 ± 0.3	6.4 ± 0.7	2.7 ± 0.2	9.4 ± 0.4	2.6 ± 0.1
	K_S	3.0 ± 0.9	2.1 ± 0.3	5.1 ± 0.6	2.0 ± 0.2	3.2 ± 0.2	2.0 ± 0.1
$K_\mathrm{S}K_\mathrm{S}$	$K_\mathrm{S}F$	5.0 ± 1.0	2.1 ± 0.5	4.2 ± 0.4	1.9 ± 0.1	4.7 ± 0.2	1.98 ± 0.05
	$K_\mathrm{S}S$	10.0 ± 2.0	3.3 ± 0.4	12.0 ± 1.0	2.5 ± 0.1	12.0 ± 0.4	2.20 ± 0.03

Table 5. The $\Lambda\Lambda$ production cross section by Σ^- as a function of x_F in mb

	Λ		Λ	
x_F	Copper	Carbon	Copper	Carbon
0.0–0.1	6.3 ± 0.2	1.51 ± 0.1	42.3 ± 0.9	11.8 ± 0.2
0.1–0.2	14.5 ± 0.3	3.7 ± 0.1	10.9 ± 0.2	3.4 ± 0.1
0.2–0.3	14.2 ± 0.3	4.1 ± 0.1	1.7 ± 0.1	0.55 ± 0.03
0.3–0.4	9.8 ± 0.4	2.9 ± 0.1	0.2 ± 0.04	0.06 ± 0.01
0.4–0.5	5.4 ± 0.2	1.80 ± 0.1	0.06 ± 0.03	0.01 ± 0.01
0.5–0.6	2.6 ± 0.2	1.01 ± 0.07	–	–
0.6–0.7	1.5 ± 0.2	0.49 ± 0.06	–	–
0.7–0.8	0.9 ± 0.6	0.18 ± 0.05	–	–

Table 6. The $\Lambda\Lambda$ production cross section by pions as a function of x_F in mb

	Λ		Λ	
x_F	Copper	Carbon	Copper	Carbon
0.0–0.1	2.9 ± 0.5	0.45 ± 0.09	8.4 ± 0.7	2.4 ± 0.2
0.1–0.2	3.3 ± 0.4	1.0 ± 0.1	1.6 ± 0.2	0.63 ± 0.09
0.2–0.3	2.4 ± 0.3	0.59 ± 0.08	0.3 ± 0.1	0.08 ± 0.03
0.3–0.4	1.1 ± 0.3	0.38 ± 0.08	–	–
0.4–0.5	0.4 ± 0.2	0.13 ± 0.05	–	–
0.5–0.6	0.13 ± 0.09	0.12 ± 0.06	–	–

and ε is the V^0 acceptance including reconstruction and trigger efficiencies. ε was calculated for each particle type i as a function of x_F and p_t^2. N_b is the number of in-

Table 7. The $\Lambda\Lambda$ production cross section by neutrons as a function of x_F in mb

	Λ		Λ	
x_F	Copper	Carbon	Copper	Carbon
0.0–0.1	3.3 ± 0.8	0.28 ± 0.08	13.0 ± 1.0	3.4 ± 0.3
0.1–0.2	4.9 ± 0.6	1.3 ± 0.2	2.8 ± 0.4	1.1 ± 0.2
0.2–0.3	4.4 ± 0.6	1.3 ± 0.2	0.5 ± 0.2	0.15 ± 0.06
0.3–0.4	1.9 ± 0.4	0.9 ± 0.2	0.08 ± 0.08	–
0.4–0.5	0.9 ± 0.4	0.4 ± 0.1	0.1 ± 0.1	–
0.5–0.6	0.7 ± 0.3	0.4 ± 0.1	–	–
0.6–0.7	0.4 ± 0.3	0.2 ± 0.1	–	–

Table 8. The ΛK_S production cross section by Σ^- as a function of x_F in mb

	Λ		K_S	
x_F	Copper	Carbon	Copper	Carbon
0.0–0.1	40.6 ± 0.5	11.5 ± 0.2	39.7 ± 0.4	12.4 ± 0.1
0.1–0.2	34.3 ± 0.4	10.0 ± 0.1	47.1 ± 0.4	14.8 ± 0.1
0.2–0.3	24.4 ± 0.3	7.4 ± 0.1	25.5 ± 0.4	7.6 ± 0.1
0.3–0.4	15.1 ± 0.3	5.29 ± 0.09	11.3 ± 0.4	3.5 ± 0.1
0.4–0.5	8.0 ± 0.2	3.08 ± 0.08	3.5 ± 0.2	1.31 ± 0.08
0.5–0.6	3.9 ± 0.2	1.63 ± 0.06	1.1 ± 0.1	0.47 ± 0.06
0.6–0.7	1.9 ± 0.1	0.86 ± 0.05	0.5 ± 0.1	0.17 ± 0.05
0.7–0.8	0.8 ± 0.1	0.41 ± 0.05	0.1 ± 0.1	0.03 ± 0.02

Table 9. The ΛK_S production cross section by π^- as a function of x_F in mb

	Λ		K_S	
x_F	Copper	Carbon	Copper	Carbon
0.0–0.1	21.0 ± 1.0	5.2 ± 0.3	11.2 ± 0.6	3.6 ± 0.2
0.1–0.2	12.2 ± 0.7	3.5 ± 0.2	15.9 ± 0.7	4.5 ± 0.2
0.2–0.3	6.3 ± 0.5	1.8 ± 0.2	9.2 ± 0.7	2.3 ± 0.2
0.3–0.4	2.6 ± 0.3	0.8 ± 0.1	5.7 ± 0.9	1.2 ± 0.2
0.4–0.5	0.9 ± 0.2	0.42 ± 0.07	1.9 ± 0.5	0.4 ± 0.1
0.5–0.6	0.6 ± 0.2	0.16 ± 0.05	0.4 ± 0.2	0.08 ± 0.06
0.6–0.7	0.3 ± 0.2	0.11 ± 0.05	–	0.09 ± 0.09

Table 10. The ΛK_S production cross section by neutrons as a function of x_F in mb

	Λ		K_S	
x_F	Copper	Carbon	Copper	Carbon
0.0–0.1	20.0 ± 2.0	4.3 ± 0.4	13.5 ± 0.9	3.9 ± 0.3
0.1–0.2	19.0 ± 1.0	4.9 ± 0.3	24.0 ± 1.0	7.1 ± 0.5
0.2–0.3	14.0 ± 2.0	4.6 ± 0.4	16.0 ± 1.0	4.6 ± 0.4
0.3–0.4	7.1 ± 0.7	2.2 ± 0.2	8.1 ± 1.0	2.1 ± 0.3
0.4–0.5	3.3 ± 0.5	1.3 ± 0.2	1.7 ± 0.5	0.8 ± 0.2
0.5–0.6	2.5 ± 0.6	0.5 ± 0.1	1.4 ± 0.6	0.4 ± 0.2
0.6–0.7	1.3 ± 0.5	0.3 ± 0.1	4.0 ± 2.0	0.1 ± 0.1
0.7–0.8	0.9 ± 0.6	0.1 ± 0.1	–	–

Table 11. The $\Lambda\overline{\Lambda}$ production cross section by Σ^- as a function of x_F in mb

	Λ		$\overline{\Lambda}$	
x_F	Copper	Carbon	Copper	Carbon
0.0–0.1	20.6 ± 0.5	5.9 ± 0.1	39.9 ± 0.6	12.9 ± 0.2
0.1–0.2	18.5 ± 0.3	5.7 ± 0.1	24.4 ± 0.4	7.8 ± 0.1
0.2–0.3	15.1 ± 0.3	4.8 ± 0.1	7.3 ± 0.3	2.14 ± 0.08
0.3–0.4	9.9 ± 0.3	3.35 ± 0.09	1.6 ± 0.1	0.64 ± 0.05
0.4–0.5	5.4 ± 0.2	2.01 ± 0.08	0.6 ± 0.2	0.17 ± 0.03
0.5–0.6	2.9 ± 0.2	1.18 ± 0.07	0.06 ± 0.04	0.04 ± 0.02
0.6–0.7	1.1 ± 0.2	0.48 ± 0.06	0.04 ± 0.04	0.01 ± 0.01
0.7–0.8	0.4 ± 0.1	0.35 ± 0.07	–	–

Table 12. The $\Lambda\overline{\Lambda}$ production cross section by π^- as a function of x_F in mb

	Λ		$\overline{\Lambda}$	
x_F	Copper	Carbon	Copper	Carbon
0.0–0.1	28.0 ± 2.0	7.7 ± 0.5	28.0 ± 1.0	7.8 ± 0.5
0.1–0.2	21.0 ± 1.0	5.9 ± 0.3	24.0 ± 1.0	7.1 ± 0.4
0.2–0.3	11.6 ± 0.9	2.8 ± 0.2	9.8 ± 0.9	2.7 ± 0.3
0.3–0.4	4.9 ± 0.6	1.6 ± 0.2	4.2 ± 0.7	1.3 ± 0.2
0.4–0.5	1.4 ± 0.4	0.8 ± 0.2	1.7 ± 0.5	0.19 ± 0.08
0.5–0.6	0.8 ± 0.3	0.22 ± 0.09	0.5 ± 0.3	0.3 ± 0.1
0.6–0.7	0.2 ± 0.2	0.06 ± 0.06	–	–

Table 13. The $\Lambda\overline{\Lambda}$ production cross section by neutrons as a function of x_F in mb

	Λ		$\overline{\Lambda}$	
x_F	Copper	Carbon	Copper	Carbon
0.0–0.1	8.0 ± 1.0	2.8 ± 0.4	15.0 ± 1.0	4.2 ± 0.4
0.1–0.2	$11. \pm 1.0$	2.5 ± 0.3	12.0 ± 1.0	3.5 ± 0.3
0.2–0.3	8.0 ± 2.0	1.9 ± 0.2	4.2 ± 0.7	1.3 ± 0.3
0.3–0.4	4.0 ± 0.7	1.7 ± 0.3	0.6 ± 0.3	0.3 ± 0.1
0.4–0.5	2.3 ± 0.6	0.7 ± 0.2	0.5 ± 0.3	0.4 ± 0.2
0.5–0.6	0.9 ± 0.4	0.5 ± 0.2	0.2 ± 0.2	0.2 ± 0.2

Table 14. The $K_S K_S$ production cross section by Σ^- as a function of x_F in mb

	K_S		K_S	
x_F	Copper	Carbon	Copper	Carbon
0.0–0.1	1.83 ± 0.05	0.52 ± 0.02	14.0 ± 0.2	4.14 ± 0.07
0.1–0.2	8.7 ± 0.1	2.59 ± 0.04	11.9 ± 0.2	3.70 ± 0.07
0.2–0.3	9.3 ± 0.2	2.63 ± 0.05	2.9 ± 0.2	0.83 ± 0.04
0.3–0.4	5.6 ± 0.2	1.81 ± 0.06	0.43 ± 0.09	0.14 ± 0.04
0.4–0.5	2.3 ± 0.2	0.77 ± 0.05	0.02 ± 0.02	–
0.5–0.6	1.1 ± 0.1	0.31 ± 0.03	–	–
0.6–0.7	0.32 ± 0.07	0.12 ± 0.02	–	–
0.7–0.8	0.11 ± 0.06	0.05 ± 0.03	–	–

Table 15. The K_SK_S production cross section by π^- as a function of x_F in mb

	K_S		K_S	
x_F	Copper	Carbon	Copper	Carbon
0.0–0.1	1.7 ± 0.2	0.44 ± 0.05	12.1 ± 0.7	3.1 ± 0.2
0.1–0.2	8.4 ± 0.4	2.5 ± 0.1	11.9 ± 0.7	3.9 ± 0.2
0.2–0.3	9.2 ± 0.6	2.6 ± 0.2	4.1 ± 0.6	1.0 ± 0.2
0.3–0.4	6.8 ± 0.7	1.5 ± 0.2	0.3 ± 0.2	0.11 ± 0.06
0.4–0.5	1.5 ± 0.3	0.8 ± 0.1	–	–
0.5–0.6	0.6 ± 0.3	0.25 ± 0.09	–	–
0.6–0.7	0.4 ± 0.3	0.10 ± 0.07	–	–

Table 16. The K_SK_S production cross section by neutrons as a function of x_F in mb

	K_S		K_S	
x_F	Copper	Carbon	Copper	Carbon
0.0–0.1	0.8 ± 0.1	0.22 ± 0.04	5.4 ± 0.4	1.5 ± 0.2
0.1–0.2	3.9 ± 0.3	1.11 ± 0.09	5.6 ± 0.6	2.2 ± 0.6
0.2–0.3	4.1 ± 0.4	0.9 ± 0.1	3.1 ± 0.6	0.7 ± 0.1
0.3–0.4	3.5 ± 0.5	0.9 ± 0.2	–	0.15 ± 0.09
0.4–0.5	0.9 ± 0.4	0.4 ± 0.1	–	–
0.5–0.6	0.3 ± 0.3	0.15 ± 0.09	–	–
0.6–0.7	0.6 ± 0.4	0.13 ± 0.09	–	–

Table 17. The $\overline{\Lambda}K_S$ production cross section by Σ^- as a function of x_F in mb

	$\overline{\Lambda}$		K_S	
x_F	Copper	Carbon	Copper	Carbon
0.0–0.1	9.7 ± 0.3	2.94 ± 0.09	3.6 ± 0.1	1.07 ± 0.03
0.1–0.2	4.8 ± 0.2	1.50 ± 0.06	4.9 ± 0.1	1.50 ± 0.04
0.2–0.3	1.33 ± 0.09	0.44 ± 0.03	3.5 ± 0.1	1.06 ± 0.04
0.3–0.4	0.37 ± 0.05	0.12 ± 0.02	2.4 ± 0.2	0.64 ± 0.04
0.4–0.5	0.08 ± 0.02	0.03 ± 0.01	1.1 ± 0.1	0.37 ± 0.04
0.5–0.6	0.03 ± 0.02	0.01 ± 0.01	0.34 ± 0.08	0.22 ± 0.04
0.6–0.7	–	–	0.24 ± 0.08	0.08 ± 0.03
0.7–0.8	–	–	0.1 ± 0.1	0.11 ± 0.05

Table 18. The $\overline{\Lambda}K_S$ production cross section by π^- as a function of x_F in mb

	$\overline{\Lambda}$		K_S	
x_F	Copper	Carbon	Copper	Carbon
0.0–0.1	10.0 ± 0.8	2.3 ± 0.2	6.2 ± 0.5	1.6 ± 0.1
0.1–0.2	6.5 ± 0.6	1.9 ± 0.2	7.4 ± 0.5	2.1 ± 0.2
0.2–0.3	3.3 ± 0.4	0.9 ± 0.1	4.4 ± 0.5	1.1 ± 0.1
0.3–0.4	0.6 ± 0.2	0.35 ± 0.08	1.7 ± 0.4	0.6 ± 0.1
0.4–0.5	0.3 ± 0.2	0.11 ± 0.05	0.8 ± 0.4	0.21 ± 0.09
0.5–0.6	0.2 ± 0.2	–	–	0.08 ± 0.06

Table 19. The $\overline{\Lambda}K_S$ production cross section by neutrons as a function of x_F in mb

	$\overline{\Lambda}$		K_S	
x_F	Copper	Carbon	Copper	Carbon
0.0–0.1	3.4 ± 0.5	0.9 ± 0.2	1.6 ± 0.3	0.33 ± 0.06
0.1–0.2	2.0 ± 0.3	0.9 ± 0.2	2.4 ± 0.3	0.56 ± 0.09
0.2–0.3	0.7 ± 0.2	0.4 ± 0.2	1.8 ± 0.4	0.6 ± 0.1
0.3–0.4	0.11 ± 0.08	0.02 ± 0.02	0.7 ± 0.3	0.3 ± 0.1
0.4–0.5	0.09 ± 0.09	–	–	0.2 ± 0.1

Table 20. The $\overline{\Lambda\Lambda}$ production cross section by Σ^- as a function of x_F in mb

	$\overline{\Lambda}$		$\overline{\Lambda}$	
x_F	Copper	Carbon	Copper	Carbon
0.0–0.1	0.43 ± 0.05	0.09 ± 0.01	1.02 ± 0.08	0.26 ± 0.02
0.1–0.2	0.52 ± 0.05	0.12 ± 0.01	0.13 ± 0.03	0.04 ± 0.01
0.2–0.3	0.13 ± 0.03	0.05 ± 0.01	0.01 ± 0.01	–
0.3–0.4	0.03 ± 0.02	0.02 ± 0.01	–	–

Table 21. The $\overline{\Lambda\Lambda}$ production cross section by π^- as a function of x_F in mb

	$\overline{\Lambda}$		$\overline{\Lambda}$	
x_F	Copper	Carbon	Copper	Carbon
0.0–0.1	0.2 ± 0.1	0.22 ± 0.06	0.8 ± 0.2	0.44 ± 0.08
0.1–0.2	0.5 ± 0.1	0.15 ± 0.05	0.5 ± 0.2	0.03 ± 0.02
0.2–0.3	0.4 ± 0.2	0.04 ± 0.03	0.06 ± 0.06	–
0.3–0.4	0.07 ± 0.07	0.07 ± 0.04	–	–

Table 22. The $\overline{\Lambda\Lambda}$ production cross section by neutrons as a function of x_F in mb

	$\overline{\Lambda}$		$\overline{\Lambda}$	
x_F	Copper	Carbon	Copper	Carbon
0.0–0.1	0.3 ± 0.2	0.06 ± 0.03	0.7 ± 0.3	0.06 ± 0.03
0.1–0.2	0.2 ± 0.1	0.02 ± 0.02	–	0.02 ± 0.02
0.2–0.3	0.3 ± 0.2	–	–	–

coming beam particles corrected for beam contaminations (for details see below) and for losses due to the deadtimes of the trigger and the data acquisition system. M, ρ and l are the atomic mass, the density and the length of the target, N_A is the Avogadro number. This formula is valid only if the efficiencies for the partners of a V^0V^0 pair are independent. We found no evidence for correlations of these efficiencies in our data and simulations.

Our Σ^-, π^- and neutron interaction samples contained several contaminating components [6, 8], which are discussed in the following.

Table 23. The $\Lambda\Lambda$ production cross section by Σ^- as a function of p_t^2 in mb/(GeV/c)^2

	Λ		Λ	
p_t^2	Copper	Carbon	Copper	Carbon
0.0–0.4	8.5 ± 0.2	2.45 ± 0.04	8.8 ± 0.2	2.52 ± 0.04
0.4–0.8	2.99 ± 0.08	0.89 ± 0.02	3.06 ± 0.08	0.89 ± 0.03
0.8–1.2	1.27 ± 0.05	0.36 ± 0.02	1.27 ± 0.06	0.34 ± 0.02
1.2–1.6	0.66 ± 0.04	0.18 ± 0.01	0.55 ± 0.04	0.15 ± 0.01
1.6–2.0	0.36 ± 0.03	0.069 ± 0.007	0.28 ± 0.03	0.080 ± 0.008
2.0–2.4	0.20 ± 0.02	0.056 ± 0.009	0.17 ± 0.02	0.048 ± 0.007
2.4–2.8	0.13 ± 0.02	0.025 ± 0.005	0.12 ± 0.02	0.025 ± 0.005
2.8–3.2	0.09 ± 0.02	0.022 ± 0.005	0.08 ± 0.01	0.007 ± 0.002
3.2–3.6	0.06 ± 0.01	0.009 ± 0.003	0.04 ± 0.01	0.008 ± 0.002
3.6–4.0	0.03 ± 0.01	0.002 ± 0.001	0.015 ± 0.007	0.006 ± 0.002

Table 24. The $\Lambda\Lambda$ production cross section by π^- as a function of p_t^2 in mb/(GeV/c)^2

	Λ		Λ	
p_t^2	Copper	Carbon	Copper	Carbon
0.0–0.4	1.6 ± 0.1	0.49 ± 0.05	1.7 ± 0.1	0.45 ± 0.04
0.4–0.8	0.62 ± 0.09	0.12 ± 0.02	0.6 ± 0.1	0.17 ± 0.04
0.8–1.2	0.22 ± 0.05	0.06 ± 0.02	0.20 ± 0.05	0.04 ± 0.01
1.2–1.6	0.11 ± 0.04	0.03 ± 0.01	0.06 ± 0.03	0.03 ± 0.01
1.6–2.0	0.05 ± 0.02	0.006 ± 0.004	0.03 ± 0.02	0.009 ± 0.006

Table 25. The $\Lambda\Lambda$ production cross section by neutrons as a function of p_t^2 in mb/(GeV/c)^2

	Λ		Λ	
p_t^2	Copper	Carbon	Copper	Carbon
0.0–0.4	3.5 ± 0.4	0.9 ± 0.09	3.4 ± 0.3	1.2 ± 0.1
0.4–0.8	1.1 ± 0.2	0.28 ± 0.05	1.4 ± 0.3	0.25 ± 0.05
0.8–1.2	0.6 ± 0.1	0.14 ± 0.04	0.4 ± 0.1	0.08 ± 0.02
1.2–1.6	0.27 ± 0.09	0.11 ± 0.04	0.09 ± 0.05	0.008 ± 0.008
1.6–2.0	0.08 ± 0.04	0.02 ± 0.01	0.10 ± 0.05	0.007 ± 0.007
2.0–2.4	0.03 ± 0.03	0.02 ± 0.01	0.05 ± 0.05	0.008 ± 0.008

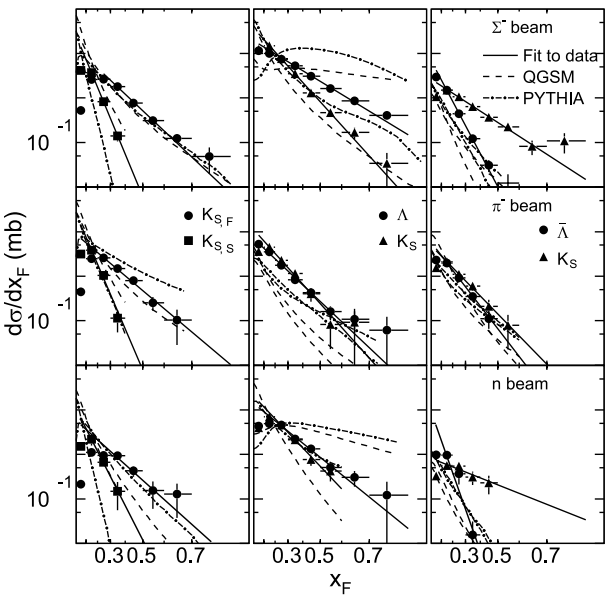

Fig. 6. Differential cross sections of inclusive K_SK_S, ΛK_S and $\overline{\Lambda}K_S$ pair production by Σ^-, π^- and neutrons in carbon, as a function of x_F (cf. Fig. 5). *Full lines*: fits to the data (see Sect. 4.2), *dotted* and *dot-dashed lines*: Monte Carlo calculations (see Sect. 6.2). The particle subscripts F and S refer to fast and slow

The Σ^- beam identified by the TRD contained about $(12.3 \pm 0.5)\%$ of fast π^-, $(2.0 \pm 0.5)\%$ of K^- and $(1.3 \pm 0.3)\%$ of Ξ^-. In the π^- sample identified by the TRD the total remaining contamination amounts to $(1.5 \pm 1)\%$, mainly Σ^-. The correction for the Σ^- contamination in the π^- interaction sample and vice versa was done iteratively. Since the contamination level in the π^- beam is quite low we used the uncorrected production cross sections measured in the π^- beam as a first level correction to the production cross section measured in the Σ^- beam. Then the corrected production cross section in the Σ^- beam was used for the corrections for π^- beam. This procedure converged after two iterations.

The cross sections for V^0 production in Ξ^- induced interactions have never been measured. Instead we used our measured cross section for production by Σ^- [1]. We suppose that the following approximate relations between the cross sections can be used:

1. $\sigma(\Xi \to \Lambda) = 2\sigma(\Sigma \to \Lambda)$ and $\sigma(\Xi \to K_S) = 2\sigma(\Sigma \to K_S)$ since the production is dominated by the strange quark fragmentation and the initial state Ξ^- contains twice as many s-quarks as Σ^-.
2. $\sigma(\Xi^- \to \overline{\Lambda}) = \sigma(\Sigma^- \to \overline{\Lambda})$ since the final state antiquarks are all new, thus the quark content of the initial state is unimportant.

The Σ^- interaction sample also contains a K^- contamination of $(2.0 \pm 0.5)\%$. The V^0 production cross sections

Table 26. The $\Lambda\overline{\Lambda}$ production cross section by Σ^- as a function of p_t^2 in mb/(GeV/c)^2

	Λ		$\overline{\Lambda}$	
p_t^2	Copper	Carbon	Copper	Carbon
0.0–0.4	11.3 ± 0.1	3.76 ± 0.05	11.7 ± 0.1	3.89 ± 0.05
0.4–0.8	4.07 ± 0.09	1.30 ± 0.03	3.91 ± 0.09	1.22 ± 0.03
0.8–1.2	1.62 ± 0.06	0.49 ± 0.02	1.53 ± 0.06	0.43 ± 0.02
1.2–1.6	0.71 ± 0.04	0.19 ± 0.01	0.67 ± 0.04	0.22 ± 0.01
1.6–2.0	0.39 ± 0.03	0.11 ± 0.01	0.43 ± 0.05	0.12 ± 0.01
2.0–2.4	0.22 ± 0.03	0.040 ± 0.006	0.16 ± 0.02	0.039 ± 0.006
2.4–2.8	0.12 ± 0.02	0.039 ± 0.006	0.12 ± 0.02	0.027 ± 0.005
2.8–3.2	0.08 ± 0.01	0.018 ± 0.004	0.06 ± 0.01	0.021 ± 0.004
3.2–3.6	0.029 ± 0.009	0.011 ± 0.003	0.04 ± 0.01	0.006 ± 0.002
3.6–4.0	0.038 ± 0.011	0.007 ± 0.003	0.012 ± 0.006	0.003 ± 0.001

Table 27. The $\Lambda\overline{\Lambda}$ production cross section by π^- as a function of p_t^2 in mb/(GeV/c)^2

	Λ		$\overline{\Lambda}$	
p_t^2	Copper	Carbon	Copper	Carbon
0.0–0.4	10.5 ± 0.4	3.1 ± 0.1	10.7 ± 0.4	3.0 ± 0.1
0.4–0.8	3.6 ± 0.3	0.93 ± 0.08	3.3 ± 0.3	0.99 ± 0.08
0.8–1.2	1.4 ± 0.2	0.37 ± 0.05	1.7 ± 0.2	0.44 ± 0.05
1.2–1.6	0.8 ± 0.1	0.17 ± 0.03	0.7 ± 0.1	0.15 ± 0.03
1.6–2.0	0.33 ± 0.09	0.09 ± 0.03	0.26 ± 0.08	0.04 ± 0.02
2.0–2.4	0.17 ± 0.06	0.06 ± 0.03	0.28 ± 0.08	0.03 ± 0.01
2.4–2.8	0.08 ± 0.04	0.04 ± 0.02	0.03 ± 0.02	0.02 ± 0.01
2.8–3.2	0.04 ± 0.03	0.02 ± 0.02	0.03 ± 0.03	0.02 ± 0.01
3.2–3.6	0.06 ± 0.04	0.02 ± 0.02	–	–

Table 28. The $\Lambda\overline{\Lambda}$ production cross section by neutrons as a function of p_t^2 in mb/(GeV/c)^2

	Λ		$\overline{\Lambda}$	
p_t^2	Copper	Carbon	Copper	Carbon
0.0–0.4	5.6 ± 0.4	1.6 ± 0.1	6.6 ± 0.7	1.8 ± 0.1
0.4–0.8	2.2 ± 0.3	0.57 ± 0.08	2.4 ± 0.3	0.44 ± 0.06
0.8–1.2	0.8 ± 0.2	0.26 ± 0.05	0.5 ± 0.1	0.23 ± 0.05
1.2–1.6	0.35 ± 0.09	0.06 ± 0.03	0.29 ± 0.09	0.06 ± 0.03
1.6–2.0	0.21 ± 0.09	0.04 ± 0.02	0.26 ± 0.09	0.06 ± 0.03
2.0–2.4	0.10 ± 0.06	0.05 ± 0.03	0.03 ± 0.03	0.02 ± 0.01

by K^- have been measured at beam momenta of up to 200 GeV/c [9] and these values were used for the correction.

Ξ^- decays upstream of the target are a source of Λ contamination in the neutron interaction sample. Since Σ^- and Ξ^- of equal momenta have practically equal decay lengths, the ratio of Λ to neutron flux is the same as the ratio of Ξ^- to Σ^- flux, i.e. 1.3% (see above). The production cross section of Λ by Λ is not known, therefore we used the production cross section of Σ^- by Σ^- measured in our experiment [10]. The resulting correction to the Λ production cross section amounts to 4%. For $\overline{\Lambda}$ and K_S this correction is negligible.

To estimate the uncertainties of the integrated cross sections we repeated the analysis with different sets of cuts applied for the V^0 identification. We changed the fiducial volume for the V^0 decays, the requirement on the dis-

Table 29. The ΛK_S production cross section by Σ^- as a function of p_t^2 in mb/(GeV/c)^2

	Λ		K_S	
p_t^2	Copper	Carbon	Copper	Carbon
0.0–0.4	19.3 ± 0.2	6.23 ± 0.05	16.6 ± 0.1	5.44 ± 0.05
0.4–0.8	6.9 ± 0.1	2.19 ± 0.03	8.4 ± 0.1	2.68 ± 0.04
0.8–1.2	2.89 ± 0.07	0.83 ± 0.02	3.42 ± 0.08	0.97 ± 0.02
1.2–1.6	1.38 ± 0.05	0.38 ± 0.02	1.58 ± 0.06	0.44 ± 0.02
1.6–2.0	0.64 ± 0.03	0.17 ± 0.01	0.85 ± 0.04	0.21 ± 0.01
2.0–2.4	0.38 ± 0.03	0.100 ± 0.008	0.41 ± 0.03	0.12 ± 0.01
2.4–2.8	0.19 ± 0.02	0.051 ± 0.006	0.27 ± 0.03	0.069 ± 0.007
2.8–3.2	0.12 ± 0.01	0.039 ± 0.007	0.18 ± 0.02	0.043 ± 0.006
3.2–3.6	0.09 ± 0.01	0.023 ± 0.004	0.14 ± 0.02	0.036 ± 0.006
3.6–4.0	0.05 ± 0.01	0.015 ± 0.003	0.09 ± 0.02	0.019 ± 0.004

Table 30. The ΛK_S production cross section by π^- as a function of p_t^2 in mb/(GeV/c)^2

	Λ		K_S	
p_t^2	Copper	Carbon	Copper	Carbon
0.0–0.4	6.7 ± 0.3	1.95 ± 0.08	5.5 ± 0.2	1.65 ± 0.07
0.4–0.8	2.4 ± 0.2	0.62 ± 0.05	3.1 ± 0.2	0.78 ± 0.06
0.8–1.2	0.8 ± 0.1	0.23 ± 0.03	1.2 ± 0.1	0.29 ± 0.03
1.2–1.6	0.43 ± 0.08	0.09 ± 0.02	0.51 ± 0.09	0.11 ± 0.02
1.6–2.0	0.4 ± 0.1	0.04 ± 0.01	0.15 ± 0.04	0.09 ± 0.02
2.0–2.4	0.14 ± 0.04	0.03 ± 0.01	0.12 ± 0.05	0.05 ± 0.01
2.4–2.8	0.12 ± 0.04	0.014 ± 0.007	0.13 ± 0.04	0.017 ± 0.008
2.8–3.2	0.04 ± 0.03	–	0.14 ± 0.07	0.013 ± 0.008
3.2–3.6	0.09 ± 0.04	0.007 ± 0.007	–	–

Table 31. The ΛK_S production cross section by neutrons as a function of p_t^2 in mb/(GeV/c)^2

	Λ		K_S	
p_t^2	Copper	Carbon	Copper	Carbon
0.0–0.4	9.7 ± 0.5	3.0 ± 0.1	10.2 ± 0.6	2.8 ± 0.2
0.4–0.8	4.3 ± 0.4	1.2 ± 0.1	4.5 ± 0.4	1.4 ± 0.1
0.8–1.2	1.7 ± 0.3	0.48 ± 0.06	1.2 ± 0.2	0.41 ± 0.06
1.2–1.6	0.5 ± 0.1	0.13 ± 0.03	0.9 ± 0.2	0.12 ± 0.03
1.6–2.0	0.5 ± 0.1	0.11 ± 0.03	0.25 ± 0.08	0.03 ± 0.01
2.0–2.4	0.17 ± 0.08	0.03 ± 0.02	0.3 ± 0.1	0.11 ± 0.04
2.4–2.8	0.05 ± 0.03	0.02 ± 0.01	0.05 ± 0.04	0.013 ± 0.008
2.8–3.2	0.04 ± 0.03	0.009 ± 0.009	0.14 ± 0.07	0.008 ± 0.008
3.2–3.6	0.02 ± 0.02	–	0.01 ± 0.01	–

Table 32. The $K_S K_S$ production cross section by Σ^- as a function of p_t^2 in mb/(GeV/c)^2

	K_S		K_S	
p_t^2	Copper	Carbon	Copper	Carbon
0.0–0.4	3.42 ± 0.05	1.05 ± 0.02	3.86 ± 0.06	1.24 ± 0.02
0.4–0.8	2.04 ± 0.05	0.61 ± 0.01	1.86 ± 0.05	0.54 ± 0.01
0.8–1.2	0.79 ± 0.03	0.23 ± 0.01	0.78 ± 0.03	0.188 ± 0.008
1.2–1.6	0.39 ± 0.02	0.117 ± 0.007	0.31 ± 0.02	0.085 ± 0.006
1.6–2.0	0.19 ± 0.02	0.052 ± 0.005	0.19 ± 0.02	0.038 ± 0.004
2.0–2.4	0.13 ± 0.02	0.038 ± 0.008	0.06 ± 0.01	0.024 ± 0.003
2.4–2.8	0.07 ± 0.01	0.014 ± 0.002	0.07 ± 0.02	0.008 ± 0.002
2.8–3.2	0.050 ± 0.009	0.008 ± 0.002	0.028 ± 0.009	0.014 ± 0.007
3.2–3.6	0.05 ± 0.01	0.010 ± 0.003	0.018 ± 0.004	0.003 ± 0.001
3.6–4.0	0.03 ± 0.01	0.005 ± 0.002	0.015 ± 0.005	–

Table 33. The $K_S K_S$ production cross section by π^- as a function of p_t^2 in mb/(GeV/c)^2

	K_S		K_S	
p_t^2	Copper	Carbon	Copper	Carbon
0.0–0.4	3.6 ± 0.2	1.04 ± 0.05	4.1 ± 0.2	1.29 ± 0.06
0.4–0.8	1.9 ± 0.1	0.53 ± 0.04	1.9 ± 0.1	0.46 ± 0.04
0.8–1.2	0.64 ± 0.09	0.21 ± 0.03	0.56 ± 0.09	0.16 ± 0.03
1.2–1.6	0.33 ± 0.08	0.09 ± 0.02	0.16 ± 0.04	0.06 ± 0.01
1.6–2.0	0.24 ± 0.06	0.06 ± 0.02	0.11 ± 0.04	0.027 ± 0.008
2.0–2.4	0.04 ± 0.02	0.021 ± 0.008	0.12 ± 0.04	0.020 ± 0.008
2.4–2.8	0.16 ± 0.05	0.02 ± 0.01	0.04 ± 0.02	0.003 ± 0.003
2.8–3.2	0.06 ± 0.03	0.018 ± 0.008	0.02 ± 0.02	0.006 ± 0.006
3.2–3.6	0.05 ± 0.04	0.003 ± 0.003	0.05 ± 0.02	–
3.6–4.0	0.01 ± 0.01	0.011 ± 0.007	0.03 ± 0.03	–

tance between tracks at the V^0 decay vertex and the allowed range for the reconstructed invariant V^0 mass. For the modified cuts the cross section result changed between -3.5 and 5.5%.

We also varied the requirements on the quality of the interaction point. With different cuts on the distance between the beam track and the reconstructed main vertex and on the distance between the tracks used in the main vertex fit, variations of the final cross section result of $\pm 4\%$ were observed.

The systematics of the trigger simulation were studied by comparing the response of the detector elements involved in the trigger for beam trigger events with an identified V^0 and for simulated events of the same type. The

Table 34. The $K_S K_S$ production cross section by neutrons as a function of p_t^2 in mb/(GeV/c)^2

	K_S		K_S	
p_t^2	Copper	Carbon	Copper	Carbon
0.0–0.4	2.5 ± 0.2	0.68 ± 0.07	2.6 ± 0.2	1.1 ± 0.2
0.4–0.8	1.3 ± 0.2	0.6 ± 0.2	1.4 ± 0.2	0.37 ± 0.06
0.8–1.2	0.6 ± 0.1	0.15 ± 0.03	0.5 ± 0.1	0.09 ± 0.03
1.2–1.6	0.30 ± 0.08	0.06 ± 0.02	0.4 ± 0.1	0.04 ± 0.01
1.6–2.0	0.1 ± 0.04	0.03 ± 0.01	0.1 ± 0.1	0.003 ± 0.003
2.0–2.4	0.1 ± 0.05	0.02 ± 0.02	–	–

Table 35. The $\overline{\Lambda\Lambda}$ production cross section by Σ^- as a function of p_t^2 in mb/(GeV/c)^2

	$\overline{\Lambda}$		$\overline{\Lambda}$	
p_t^2	Copper	Carbon	Copper	Carbon
0.0–0.4	0.18 ± 0.02	0.047 ± 0.005	0.18 ± 0.02	0.056 ± 0.005
0.4–0.8	0.06 ± 0.01	0.018 ± 0.003	0.07 ± 0.01	0.010 ± 0.002
0.8–1.2	0.019 ± 0.005	0.007 ± 0.002	0.024 ± 0.006	0.005 ± 0.002
1.2–1.6	0.019 ± 0.006	0.002 ± 0.001	0.022 ± 0.006	0.002 ± 0.001
1.6–2.0	0.005 ± 0.003	–	0.002 ± 0.002	0.002 ± 0.001
2.0–2.4	0.004 ± 0.003	–	0.003 ± 0.003	–

Table 36. The $\overline{\Lambda\Lambda}$ production cross section by π^- as a function of p_t^2 in mb/(GeV/c)^2

	$\overline{\Lambda}$		$\overline{\Lambda}$	
p_t^2	Copper	Carbon	Copper	Carbon
0.0–0.4	0.15 ± 0.04	0.092 ± 0.02	0.22 ± 0.06	0.091 ± 0.02
0.4–0.8	0.12 ± 0.05	–	0.06 ± 0.03	0.02 ± 0.01
0.8–1.2	0.03 ± 0.02	0.013 ± 0.008	–	0.004 ± 0.004
1.2–1.6	0.03 ± 0.02	0.014 ± 0.008	–	–

Table 37. The $\overline{\Lambda\Lambda}$ production cross section by neutrons as a function of p_t^2 in mb/(GeV/c)^2

	$\overline{\Lambda}$		$\overline{\Lambda}$	
p_t^2	Copper	Carbon	Copper	Carbon
0.0–0.4	0.3 ± 0.1	0.03 ± 0.02	0.3 ± 0.1	0.04 ± 0.02
0.4–0.8	–	–	0.04 ± 0.04	–

simulated trigger reproduces the trigger response found in real events within ±7%. A small dependence on the general event multiplicity was found. We therefore assigned a total systematic error of $\sigma = 10\%$ to the uncertainties in the trigger efficiency.

The time dependence of the detector and trigger efficiencies showed variations corresponding to an uncertainty of $\sigma \approx 2\%$.

We attribute a total systematic error of $\sigma = 15\%$ to all measured cross sections, taking into account the possibility of correlations between the different contributions. In order to conserve the information on the x_F and p_t dependence of the cross sections we did not include these systematic errors into the cross section tables given in the following section.

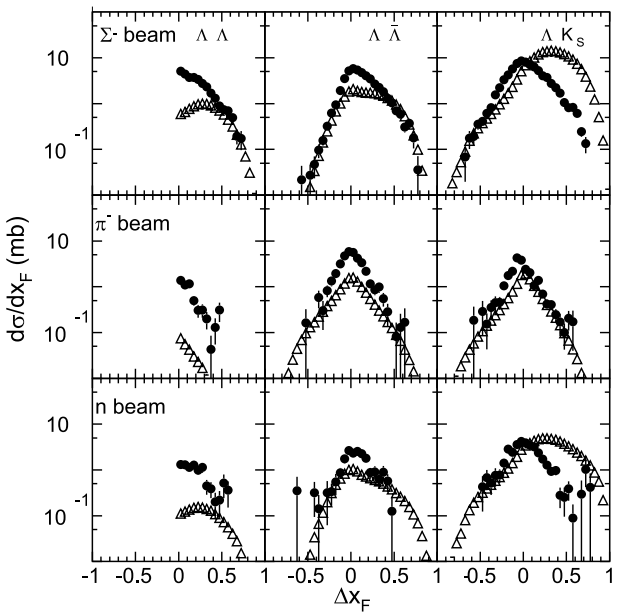

Fig. 7. Differential cross sections of inclusive $\Lambda\Lambda$, $\Lambda\overline{\Lambda}$ and ΛK_S pair production by Σ^-, π^- and neutrons in carbon as a function of Δx_F. Only statistical errors are shown. • – data, △ – calculation by PYTHIA

Table 38. The $\overline{\Lambda}K_S$ production cross section by Σ^- as a function of p_t^2 in mb/(GeV/c)^2

	$\overline{\Lambda}$		K_S	
p_t^2	Copper	Carbon	Copper	Carbon
0.0–0.4	2.62 ± 0.07	0.84 ± 0.02	2.08 ± 0.05	0.68 ± 0.02
0.4–0.8	0.79 ± 0.04	0.25 ± 0.01	1.09 ± 0.04	0.33 ± 0.02
0.8–1.2	0.31 ± 0.02	0.086 ± 0.007	0.50 ± 0.05	0.14 ± 0.01
1.2–1.6	0.18 ± 0.02	0.038 ± 0.005	0.18 ± 0.02	0.052 ± 0.006
1.6–2.0	0.08 ± 0.01	0.030 ± 0.005	0.10 ± 0.02	0.026 ± 0.004
2.0–2.4	0.034 ± 0.007	0.007 ± 0.002	0.054 ± 0.009	0.011 ± 0.003
2.4–2.8	0.036 ± 0.007	0.006 ± 0.002	0.04 ± 0.01	0.003 ± 0.001
2.8–3.2	0.018 ± 0.006	0.005 ± 0.002	0.014 ± 0.006	0.005 ± 0.002
3.2–3.6	0.007 ± 0.004	0.001 ± 0.001	0.007 ± 0.004	0.005 ± 0.002
3.6–4.0	0.003 ± 0.002	0.001 ± 0.001	0.008 ± 0.004	0.002 ± 0.001

Table 39. The $\overline{\Lambda}K_S$ production cross section by π^- as a function of p_t^2 in mb/(GeV/c)^2

	$\overline{\Lambda}$		K_S	
p_t^2	Copper	Carbon	Copper	Carbon
0.0–0.4	4.5 ± 0.3	1.37 ± 0.09	3.7 ± 0.2	1.07 ± 0.07
0.4–0.8	1.7 ± 0.2	0.35 ± 0.04	1.8 ± 0.2	0.56 ± 0.06
0.8–1.2	0.6 ± 0.1	0.16 ± 0.03	0.7 ± 0.1	0.18 ± 0.03
1.2–1.6	0.18 ± 0.05	0.10 ± 0.03	0.48 ± 0.09	0.09 ± 0.03
1.6–2.0	0.20 ± 0.07	0.02 ± 0.01	0.11 ± 0.04	0.04 ± 0.02
2.0–2.4	0.03 ± 0.02	0.006 ± 0.006	0.09 ± 0.05	0.04 ± 0.02
2.4–2.8	0.02 ± 0.02	0.007 ± 0.005	0.08 ± 0.06	0.04 ± 0.02
2.8–3.2	–	0.004 ± 0.004	0.06 ± 0.05	–

Table 40. The $\overline{\Lambda}K_S$ production cross section by neutrons as a function of p_t^2 in mb/(GeV/c)^2

	$\overline{\Lambda}$		K_S	
p_t^2	Copper	Carbon	Copper	Carbon
0.0–0.4	0.8 ± 0.1	0.40 ± 0.06	0.62 ± 0.07	0.34 ± 0.05
0.4–0.8	0.29 ± 0.06	0.17 ± 0.04	0.33 ± 0.08	0.16 ± 0.04
0.8–1.2	0.06 ± 0.03	0.05 ± 0.03	0.15 ± 0.05	0.09 ± 0.04
1.2–1.6	0.04 ± 0.02	0.02 ± 0.01	0.07 ± 0.03	0.03 ± 0.01
1.6–2.0	0.02 ± 0.02	0.004 ± 0.004	0.07 ± 0.04	0.008 ± 0.008

4.2 Results

The total production cross sections per nucleus for $x_{F,1} > 0$, $x_{F,2} > 0$ and all p_t^2 are listed in Table 1 for the different V^0V^0 combinations, beam particles and targets.

The ratio of the cross sections for the copper and carbon targets varies from 3.2 to 3.9 and shows no significant dependence on the type of beam particle or V^0, with the possible exception that the ratio for production by Σ^- is lower for all pairs except $\Lambda\Lambda$. Assuming the nuclear dependence of the cross sections to be $\sigma_A \propto A^\alpha$, the range of ratios corresponds to $\alpha = 0.74 \pm 0.03$.

The differential production cross sections as a function of x_F and p_t^2 were calculated for the individual partners of the V^0V^0 pairs. They are shown in Figs. 5–6 for x_F and the carbon data. The data for both the copper and carbon targets are listed in Tables 5–40 for x_F and p_t^2. In the $\Lambda\Lambda$, K_SK_S and $\overline{\Lambda}\overline{\Lambda}$ pairs we sorted the partners by their x_F value, referring to them as V_F^0 for the faster and V_S^0 for the slower partner. We also measured the differential production cross section as a function of the difference $\Delta x_F = x_F(\text{fast}) - x_F(\text{slow})$. The results are shown in Figs. 7–8 and Tables 41–46. The error bars in the plots and the errors listed in the tables correspond to the statistical errors only.

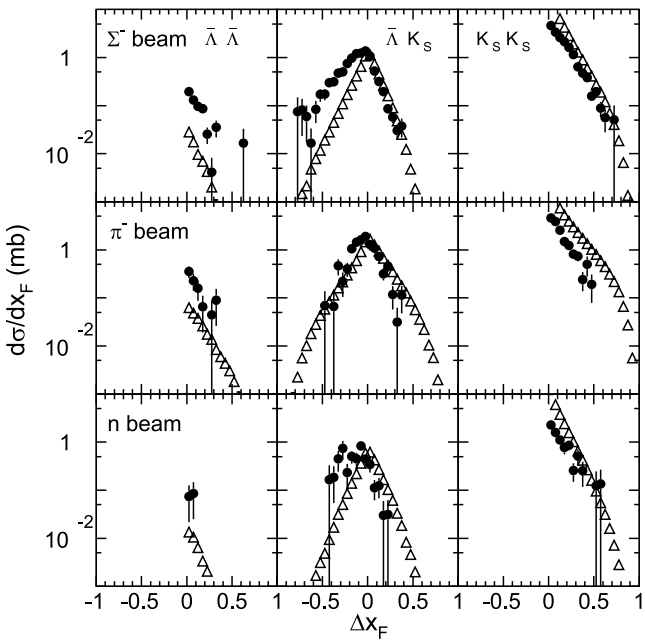

Fig. 8. Differential cross sections of inclusive $\Lambda\overline{\Lambda}$, $\overline{\Lambda}K_S$ and K_SK_S pair production by Σ^-, π^- and neutrons in carbon as a function of Δx_F. Only statistical errors are shown. • – data, △ – calculation by PYTHIA

Table 41. The $\Lambda\Lambda$ production cross section as a function of Δx_{F} in mb

	neutrons		π^-		Σ^-	
x_{F}	Copper	Carbon	Copper	Carbon	Copper	Carbon
0.0–0.1	8.0 ± 8.0	1.3 ± 0.5	6.0 ± 8.0	1.3 ± 0.5	$18. \pm 0.6$	4.7 ± 0.4
0.1–0.2	4.0 ± 1.0	1.2 ± 0.5	2.5 ± 0.5	0.9 ± 0.4	13.5 ± 0.5	3.8 ± 0.4
0.2–0.3	2.5 ± 1.0	1.1 ± 0.5	1.5 ± 0.5	0.3 ± 0.3	10.0 ± 0.5	3.1 ± 0.4
0.3–0.4	1.5 ± 1.0	0.4 ± 0.4	0.5 ± 0.5	0.1 ± 0.3	7.5 ± 0.5	2.0 ± 0.3
0.4–0.5	0.5 ± 0.5	0.2 ± 0.4	0.2 ± 0.4	0.2 ± 0.4	3.5 ± 0.5	1.1 ± 0.3
0.5–0.6	0.3 ± 0.5	0.5 ± 0.5	–	–	1.8 ± 0.5	0.7 ± 0.3
0.6–0.7	0.3 ± 0.5	–	–	–	1.0 ± 0.0	0.4 ± 0.3
0.7–0.8	–	–	–	–	0.5 ± 0.5	0.1 ± 0.2

Table 42. The $\Lambda\overline{\Lambda}$ production cross section as a function of Δx_{F} in mb

	neutrons		π^-		Σ^-	
x_{F}	Copper	Carbon	Copper	Carbon	Copper	Carbon
(-0.6)–(-0.5)	–	–	0.3 ± 0.5	0.1 ± 0.3	–	0.01 ± 0.1
(-0.5)–(-0.4)	0.3 ± 0.1	0.2 ± 0.4	0.2 ± 0.4	–	0.3 ± 0.5	0.04 ± 0.2
(-0.4)–(-0.3)	0.2 ± 0.5	0.05 ± 0.3	1.5 ± 0.5	0.5 ± 0.5	0.4 ± 0.3	0.2 ± 0.2
(-0.3)–(-0.2)	1.3 ± 0.5	0.4 ± 0.5	4.0 ± 1.0	1.1 ± 0.5	1.1 ± 0.4	0.5 ± 0.3
(-0.2)–(-0.1)	2.0 ± 1.0	0.5 ± 0.5	9.0 ± 1.0	2.5 ± 0.5	5.1 ± 0.5	1.5 ± 0.3
(-0.1)–(0.0)	8.0 ± 1.0	2.5 ± 0.5	19.0 ± 2.0	5.4 ± 0.5	14.5 ± 0.5	4.4 ± 0.4
0.0–0.1	8.0 ± 1.0	2.5 ± 0.5	18.0 ± 1.0	5.1 ± 0.5	19.0 ± 0.5	5.6 ± 0.4
0.1–0.2	5.0 ± 1.0	2.5 ± 0.5	10.0 ± 1.0	3.0 ± 0.5	13.5 ± 0.5	4.4 ± 0.4
0.2–0.3	4.0 ± 1.0	1.1 ± 0.5	5.0 ± 1.0	1.0 ± 0.5	9.5 ± 0.5	3.1 ± 0.4
0.3–0.4	2.0 ± 1.0	1.0 ± 0.5	1.0 ± 0.5	0.8 ± 0.5	5.0 ± 0.5	2.1 ± 0.4
0.4–0.5	1.1 ± 0.5	0.4 ± 0.5	1.0 ± 0.5	0.2 ± 0.3	3.1 ± 0.5	1.2 ± 0.4
0.5–0.6	0.2 ± 0.5	–	0.2 ± 0.4	0.1 ± 0.4	1.6 ± 0.5	0.7 ± 0.3
0.6–0.7	–	–	–	0.1 ± 0.3	0.5 ± 0.4	0.4 ± 0.3
0.7–0.8	–	–	–	–	0.2 ± 0.4	0.1 ± 0.3

Table 43. The ΛK_{S} production cross section as a function of Δx_{F} in mb

	neutrons		π^-		Σ^-	
x_{F}	Copper	Carbon	Copper	Carbon	Copper	Carbon
(-0.7)–(-0.6)	1.0 ± 1.0	–	–	–	0.2 ± 0.4	0.1 ± 0.3
(-0.6)–(-0.5)	2.0 ± 1.0	–	0.2 ± 0.5	0.1 ± 0.3	0.5 ± 0.4	0.3 ± 0.3
(-0.5)–(-0.4)	3.0 ± 2.0	0.5 ± 0.5	0.5 ± 0.5	0.2 ± 0.4	1.3 ± 0.5	0.5 ± 0.3
(-0.4)–(-0.3)	2.0 ± 1.0	0.5 ± 0.5	3.0 ± 1.0	0.4 ± 0.4	4.0 ± 0.5	1.2 ± 0.3
(-0.3)–(-0.2)	6.0 ± 1.0	0.5 ± 0.5	5.0 ± 1.0	0.8 ± 0.4	8.9 ± 0.5	2.8 ± 0.4
(-0.2)–(-0.1)	8.0 ± 1.0	2.5 ± 0.5	8.0 ± 1.0	2.1 ± 0.5	17.0 ± 0.5	4.8 ± 0.4
(-0.1)–(0.0)	15.0 ± 1.0	4.1 ± 0.5	12.0 ± 1.0	4.0 ± 0.5	28.9 ± 0.5	8.1 ± 0.4
0.0–0.1	13.0 ± 1.0	3.5 ± 0.5	8.0 ± 1.0	2.2 ± 0.4	25.8 ± 0.5	7.6 ± 0.3
0.1–0.2	8.0 ± 1.0	3.1 ± 0.5	4.0 ± 0.5	1.2 ± 0.4	17.9 ± 0.5	5.6 ± 0.4
0.2–0.3	5.0 ± 1.0	1.6 ± 0.5	2.0 ± 0.5	0.6 ± 0.4	11.8 ± 0.5	3.7 ± 0.3
0.3–0.4	3.0 ± 1.0	0.9 ± 0.4	0.5 ± 0.5	0.4 ± 0.3	6.0 ± 0.5	2.5 ± 0.3
0.4–0.5	3.0 ± 1.0	0.3 ± 0.4	0.5 ± 0.5	0.2 ± 0.3	3.4 ± 0.5	1.4 ± 0.3
0.5–0.6	0.3 ± 0.3	0.3 ± 0.4	0.3 ± 0.5	0.2 ± 0.4	3.8 ± 0.5	0.8 ± 0.3
0.6–0.7	–	0.3 ± 0.8	–	–	1.5 ± 0.8	0.5 ± 0.3
0.7–0.8	–	0.5 ± 0.5	–	–	0.2 ± 0.4	0.06 ± 0.2

Table 44. The $\overline{\Lambda}\overline{\Lambda}$ production cross section as a function of Δx_{F} in mb

	neutrons		π^-		Σ^-	
x_{F}	Copper	Carbon	Copper	Carbon	Copper	Carbon
0.0–0.1	0.4 ± 0.4	0.1 ± 0.3	0.7 ± 0.5	0.3 ± 0.3	0.8 ± 0.3	0.2 ± 0.2
0.1–0.2	0.3 ± 0.4	–	0.3 ± 0.4	0.1 ± 0.3	0.3 ± 0.3	0.1 ± 0.1
0.2–0.3	0.1 ± 0.3	–	0.2 ± 0.4	0.02 ± 0.2	0.1 ± 0.2	0.02 ± 0.1
0.3–0.4	–	–	–	0.09 ± 0.4	0.01 ± 0.1	0.02 ± 0.1

Table 45. The $\overline{\Lambda}K_{\mathrm{S}}$ production cross section as a function of Δx_{F} in mb

	neutrons		π^-		Σ^-	
x_{F}	Copper	Carbon	Copper	Carbon	Copper	Carbon
(-0.6)–(-0.5)	–	–	–	–	0.3 ± 0.4	0.2 ± 0.2
(-0.5)–(-0.4)	–	0.1 ± 0.3	0.5 ± 0.5	0.04 ± 0.2	0.5 ± 0.4	0.3 ± 0.2
(-0.4)–(-0.3)	–	0.3 ± 0.4	0.3 ± 0.5	0.3 ± 0.4	1.0 ± 0.4	0.4 ± 0.3
(-0.3)–(-0.2)	1.5 ± 0.5	0.5 ± 0.4	2.0 ± 1.0	0.3 ± 0.3	2.3 ± 0.5	0.7 ± 0.3
(-0.2)–(-0.1)	1.1 ± 0.5	0.5 ± 0.4	4.0 ± 1.0	1.2 ± 0.5	3.6 ± 0.5	1.1 ± 0.3
(-0.1)–(0.0)	2.1 ± 0.5	0.7 ± 0.4	7.0 ± 1.0	1.8 ± 0.5	4.6 ± 0.6	1.3 ± 0.3
0.0–0.1	1.0 ± 0.5	0.3 ± 0.3	4.5 ± 0.5	1.2 ± 0.4	2.5 ± 0.4	0.8 ± 0.2
0.1–0.2	0.2 ± 0.3	0.1 ± 0.2	2.5 ± 0.5	0.5 ± 0.3	0.7 ± 0.3	0.3 ± 0.2
0.2–0.3	0.2 ± 0.3	0.02 ± 0.1	0.6 ± 0.4	0.3 ± 0.3	0.3 ± 0.2	0.05 ± 0.1
0.3–0.4	0.1 ± 0.3	–	0.1 ± 0.3	0.05 ± 0.2	0.05 ± 0.2	0.04 ± 0.1

Table 46. The $K_{\mathrm{S}}K_{\mathrm{S}}$ production cross section as a function of Δx_{F} in mb

	neutrons		π^-		Σ^-	
x_{F}	Copper	Carbon	Copper	Carbon	Copper	Carbon
0.0–0.1	7.0 ± 1.0	1.9 ± 0.5	15.0 ± 1.0	4.0 ± 0.5	14.1 ± 0.5	4.0 ± 0.3
0.1–0.2	4.5 ± 0.9	0.9 ± 0.5	8.0 ± 1.0	2.1 ± 0.5	8.0 ± 0.5	2.4 ± 0.3
0.2–0.3	2.5 ± 0.9	0.6 ± 0.4	4.0 ± 1.0	1.0 ± 0.4	4.1 ± 0.5	1.4 ± 0.3
0.3–0.4	0.5 ± 1.0	0.4 ± 0.4	1.1 ± 0.5	0.5 ± 0.4	1.7 ± 0.4	0.5 ± 0.2
0.4–0.5	–	–	0.5 ± 0.5	0.4 ± 0.4	0.9 ± 0.4	0.3 ± 0.2
0.5–0.6	0.3 ± 0.5	0.2 ± 0.4	–	–	0.4 ± 0.3	0.2 ± 0.2
0.6–0.7	–	–	–	–	0.2 ± 0.3	0.03 ± 0.1

The cross sections were parametrized by a function of the form:

$$\frac{\mathrm{d}^2\sigma}{\mathrm{d}p_{\mathrm{t}}^2\,\mathrm{d}x_{\mathrm{F}}} = C(1-x_{\mathrm{F}})^n \cdot \exp(-Bp_{\mathrm{t}}^2)\,, \qquad (2)$$

which is based on quark counting rules and phase space arguments [11]. The three parameters C, n and B were assumed to be independent of p_{t}^2 and x_{F}. While for the fit in p_{t}^2 all bins with significant statistics were used, the fits in x_{F} used only that part of the spectrum in the limited kinematic range. In this case, however, equal fit ranges were used for the carbon and copper data of a given beam particle and V^0V^0 pair combination. The values of n and B obtained from the fits are listed in Tables 3–4 for each target with the corresponding fit errors. The results of the x_{F} fits are shown in the figures as a solid straight lines over the fit range.

No significant difference between the values obtained from the copper and the carbon target was observed. The x_{F} spectra vary strongly between the different beam and V^0V^0 combinations, this will be discussed in Sect. 6.2. The p_{t}^2 spectra, on the other hand, show no significant effects of either beam particle or V^0V^0 type.

5 Mass spectra of V^0V^0 pairs

We have looked for possible resonances in the mass spectra of all V^0V^0 combinations considered, $\Lambda\Lambda$, $\Lambda\overline{\Lambda}$, ΛK_{S}, $\overline{\Lambda}\overline{\Lambda}$, $\overline{\Lambda}K_{\mathrm{S}}$ and $K_{\mathrm{S}}K_{\mathrm{S}}$. The only visible resonance peak appears in the $K_{\mathrm{S}}K_{\mathrm{S}}$ mass spectrum at around $1525\,\mathrm{MeV}/c^2$, the mass of the $f_2'(1525)$. This signal will be discussed below. We also present an upper limit on the production cross section of the possibly existing H dibaryon decaying to $\Lambda\Lambda$.

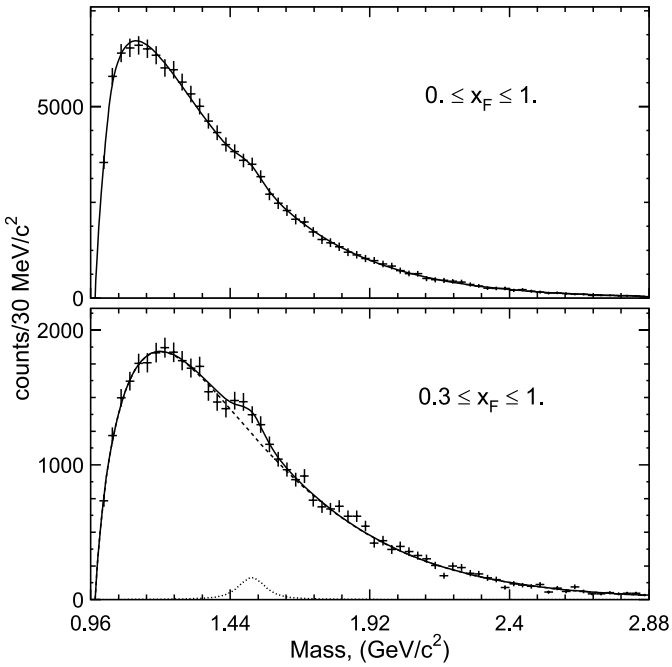

Fig. 9. Acceptance-corrected $K_{\rm S}K_{\rm S}$ invariant mass spectrum

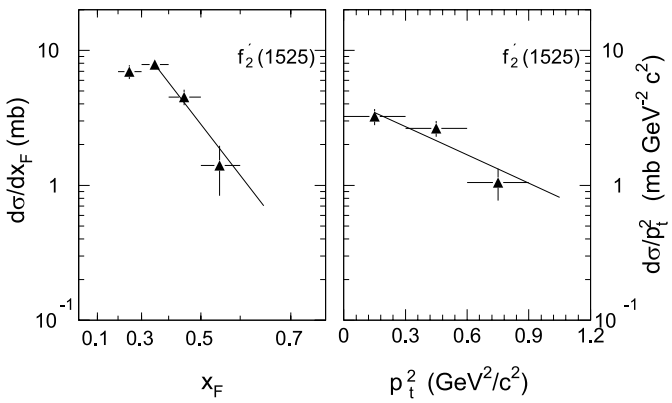

Fig. 10. $BR\cdot \mathrm{d}\sigma/\mathrm{d}x_{\rm F}$ and $BR\cdot \mathrm{d}\sigma/\mathrm{d}p_{\rm t^2}$ per Cu nucleus for inclusive production of $f_2'(1525) \to K_{\rm S}K_{\rm S}$ by Σ^-

5.1 $f_2'(1525)$ production

We have observed about $13000 K_{\rm S}K_{\rm S}$ pairs produced by Σ^- (Table 2). Their invariant mass distribution is shown in Fig. 9. The events have been weighted individually by the inverse of the detection efficiency. A clear signal in the vicinity of the tensor meson $f_2'(1525)$ is visible at higher $x_{\rm F}$. The distribution was fitted by the sum of a Gaussian for the signal and a background function whose shape was taken from 'event mixing', where the fast $K_{\rm S}$ from one event was combined with the slow $K_{\rm S}$ from a different event. The fit result was a signal of (939 ± 129) events at a mass of $M = (1516 \pm 8)\,\mathrm{MeV}/c^2$ with a width of $\Gamma = (76 \pm 25)\,\mathrm{MeV}/c^2$. The position and the width of the signal correspond to the world average values for the $f_2'(1525)$, $M = (1525 \pm 5)\,\mathrm{MeV}/c^2$ and $\Gamma = 73^{+6}_{-5}\,\mathrm{MeV}/c^2$ [12]. The product of the differential production cross section and the branching ratio to $K_{\rm S}K_{\rm S}$ as a function of $x_{\rm F}$ and $p_{\rm t}^2$ is shown in Fig. 10 and listed in Tables 47–48. The quoted errors are statistical only. The parametrization of the differential cross sections used in section 4.2 yields $n = 4 \pm 1$ and $B = 1.6 \pm 0.4$.

Table 47. The f_{1525} production cross section as a function of $x_{\rm F}$ in mb

$x_{\rm F}$	copper	carbon
0.2–0.3	6.9 ± 0.8	2.2 ± 0.3
0.3–0.4	7.8 ± 0.7	2.5 ± 0.2
0.4–0.5	4.5 ± 0.6	1.4 ± 0.2
0.5–0.6	1.4 ± 0.6	0.4 ± 0.2

Table 48. The f_{1525} production cross section as a function of $p_{\rm t}^2$ in $\mathrm{mb}/(\mathrm{GeV}/c)^2$

$p_{\rm t}^2$	copper	carbon
0.0–0.3	3.2 ± 0.4	1.0 ± 0.1
0.3–0.6	2.6 ± 0.4	0.8 ± 0.1
0.6–0.9	1.0 ± 0.3	0.3 ± 0.1

5.2 Search for the H-dibaryon

The prediction of the H mass was done within the framework of the bag model [25]. The basic idea of this relativistic model is that the quarks of the particle exist as a free and massless objects within a 'sphere' in which they are confined by an *ad hoc* introduced 'pressure' [26]. The H mass was first calculated to be $2145\,\mathrm{GeV}/c^2$, but including some corrections [27, 28] increases the mass. Within this model the hyperon masses are, however, not very well reproduced. The non relativistic quark (cluster) model [26] was more successful describing baryon masses. The calculations leads to the H mass around $2215\,\mathrm{GeV}/c^2$ [29]. More information on theoretical aspects of the H mass calculations may be found at [30].

We have searched our sample of about $12000 \Lambda\Lambda$ pairs for a signal from $\mathrm{H} \to \Lambda\Lambda$ decays. The $\Lambda\Lambda$ mass spectrum of the copper target is shown in Fig. 11. Again, the events have been weighted individually by the inverse of the detection efficiency. The solid line in a) represents the background determined from event mixing after normalization to the data. The data after subtraction of the background are shown in b). No significant signal is visible. Upper limits on the inclusive production cross section in the region $0.1 < x_{\rm F} < 0.8$ were calculated assuming a width $\Gamma_{\rm H} = 20\,\mathrm{MeV}/c^2$ and using the prescription of [13]. The results are shown Fig. 11c as a function of the $\Lambda\Lambda$ mass. Over the mass region shown, we obtained upper limits of $55 \mu b$ and $15 \mu b$ for production in the copper and carbon target, resp. Assuming an $A^{2/3}$ dependence for H-dibaryon production, we obtained an upper limit on the produc-

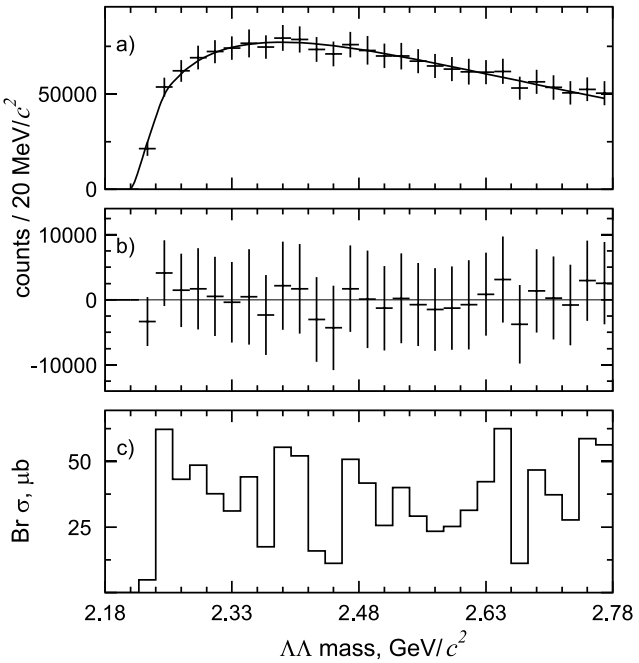

Fig. 11. Search for $H \to \Lambda\Lambda$ decays (copper target): (**a**) acceptance-corrected invariant mass distribution of $\Lambda\Lambda$ pairs and the background estimated by event mixing (*line*) (**b**) acceptance-corrected invariant mass distribution after background subtraction (**c**) upper limits (95% CL) for the production cross section assuming $\Gamma_H = 20\,\mathrm{MeV}/c^2$

tion cross section of $3\mu b$ per nucleon. This limit scales with $\sqrt{\Gamma_\mathrm{H}}$. All limits are at the 95% confidence level.

6 Discussion

6.1 Total V^0V^0 production cross sections

We remind the reader that the cross sections were measured under the requirement that both V^0 have $x_\mathrm{F} > 0$. The total cross sections listed in Table 1 exhibit large differences between different combinations of beam particles and V^0V^0 pairs. Some of these can be understood qualitatively:

The cross section for the production of $\Lambda\Lambda$ and ΛK_S pairs is larger for the Σ^- beam than for the neutron or π^- beam, which is the well-known effect of the large valence quark overlap of beam particle and produced particle – see for instance the production cross sections of Λ, Ξ^- or Ω^- by protons, Σ^- and Ξ^- compiled in Fig. 8 of [8].

For $\Lambda\overline{\Lambda}$ production, the π^- beam particle has a $\overline{u}$ valence quark overlap with the $\overline{\Lambda}$, which makes this production larger than ΛK_S production in the same beam and about equal to $\Lambda\overline{\Lambda}$ production by Σ^-.

For the same reason, $\overline{\Lambda\Lambda}$ production is larger in the π^- beam than in the Σ^- or neutron beam, but the cross sections are still very low because of the need to produce two antibaryons.

For the first time the A dependence have been measured for V^0-pair production cross section. We may only compare our value of $\alpha = 0.74 \pm 0.03$ with the results of other experiments for single V^0 production cross section in a different beams (see [1] and references therein). The measured value is close to the published one.

6.2 x_F spectra

Associated production of particles provides a deep and sensitive probe of the hadronization mechanisms, because it allows to study contributions from (nonleading) parts of the fragmentation chains, which are not accessible in studies of inclusive production.

The strong "leading particle effect" observed in the x_F-distributions of single V^0 [1] suggests two distinct production mechanisms for baryons: At high x_F valence quark or diquark transfer from the beam projectile to the produced hadrons may dominate, while at low x_F baryons are produced mainly in a soft hadronization process described e.g. by several break-ups of a colour string which is stretched between the partons.

Studying the individual x_F spectra, we note strong differences between the x_F spectra of the partners for several pair/beam combinations: in particular for $\Lambda\Lambda$ (Σ^-) and to a lesser extent in $\Lambda\overline{\Lambda}$ (Σ^-), $K_\mathrm{S}K_\mathrm{S}$ (Σ^-, n) and $\overline{\Lambda}K_\mathrm{S}$ (Σ^-). This underlines the importance of s quark transfer from the beam projectile to the hadron produced. We also note that the second Λ of $\Lambda\Lambda$ pairs has a considerably softer spectrum than the $\overline{\Lambda}$ of $\Lambda\overline{\Lambda}$ pairs, for all beams. This effect cannot be explained by quark transfer.

We have calculated the differential cross sections $\mathrm{d}\sigma/\mathrm{d}x_\mathrm{F}$ using PYTHIA [14] and the quark–gluon string model (QGSM, see [15–19] and references therein).

PYTHIA was used with its default set of parameters. Among the essential details, we only mention the inclusion of elastic and diffraction processes (PYTHIA option MSEL = 2) and the usage of the Lund string fragmentation algorithm. The latter is closer to the QGSM ansatz than "independent" or "cluster" fragmentation. In the case of inclusive single particle distributions [1], PYTHIA has demonstrated a reasonably good description of the data.

Since PYTHIA can only deal with reactions on single nucleons (not nuclei), an extrapolation to the carbon and copper targets was made according to the simple power low: $\sigma \sim A^\alpha$ with $\alpha = 2/3$. However, if started from a single proton, this formula is known to underestimate the total reaction rate by about a factor of 1.5 to 2, as observed in an earlier hyperon beam experiment at CERN [20]. As the evaluation of this factor can only be based on an independent experimental measurement or still another theoretical model, the corresponding correction has not been included in the curves shown in Figs. 7–8.

The adaptation of the quark–gluon string model to two-particle events needs some explanations. Normally, the model is assumed to consider only inclusive single particle spectra, with all accompanying particles absorbed into a 'reggeized' state in the exchange channel. Therefore, the model cannot predict real interparticle correlations. However, the problem may be reformulated in a slightly different way. One can consider the inclusive single particle dis-

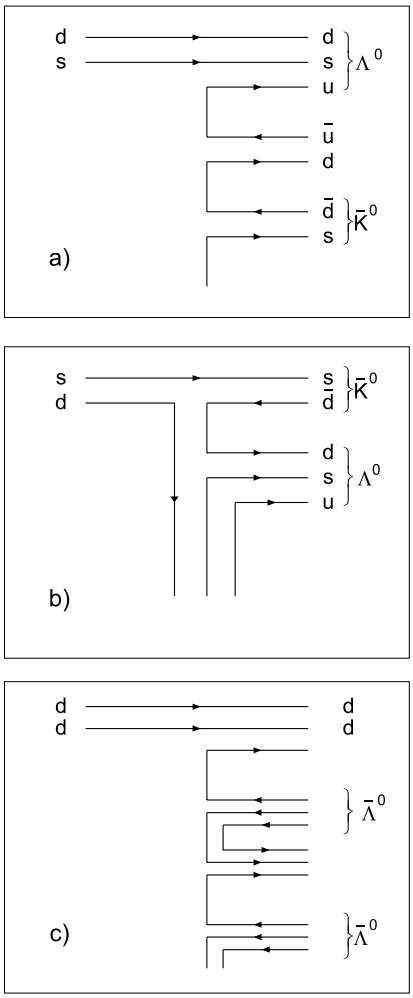

Fig. 12. The parton fragmentation diagrams used in the QGSM model for two-particle production

tribution under the requirement that another definite particle appears in the parton fragmentation diagram. Some typical examples of such diagrams are shown in Fig. 12a–c. Note that the production of a pair of particles may proceed via different fragmentation steps. In the example shown in Fig. 12c, the leading particle may be either $\overline{K}$ or Λ, and both these diagrams must be taken into account. The corresponding fragmentation functions obey the same quark counting rules as those exploited in our earlier analyses (where only the leading particles have been considered in each case). The complete set of extended fragmentation functions is, obviously, too long to be presented in this paper, but is obtainable as a part of the HIPPOPO code [21, 22].[2]

As in the case of single particle distributions, the absolute normalization of the cross sections is not predictable within the Quark-Gluon String Model itself, and the relevant normalizing factors have to be taken as phenomenological parameters. On the contrary, the predictions made by PYTHIA include the normalization. PYTHIA generally understimates the production cross sections for $\Lambda\Lambda$, $\Lambda\overline{\Lambda}$ and $\overline{\Lambda}\overline{\Lambda}$, in the case of $\Lambda\Lambda$ production by π^- by more than one order of magnitude.

There are also important differences between the $x_{\rm F}$ distributions in the data and the predictions from PYTHIA and the QGSM: Both models overestimate the leading behaviour of the Λ in the $\Lambda K_{\rm S}$ pairs produced by Σ^- and neutrons. We found the same behaviour in the inclusive production of single Λ [1]. On the other hand, in the production of $\overline{\Lambda}K_{\rm S}$ pairs by Σ^- and neutrons, both models fail to reproduce the strong leading particle effect seen for the $K_{\rm S}$. It may be worth pointing out that the experimental spectrum of $K_{\rm S}$ produced in association with an $\overline{\Lambda}$ is harder than the spectrum of $K_{\rm S}$ produced inclusively, see [1].

In summary it can be said that both models have problems to describe the leading particle effect and that for some pair productions the magnitude of the cross sections predicted by PYTHIA is far too low.

6.3 f_2' production

No other cross section measurements exist for inclusive f_2' production in high-energy hadronic reactions. Our value of $\sigma(x_{\rm F} > 0.2) = (130 \pm 25)\mu b$ *per nucleon* is larger by more than one order of magnitude than the cross section for $\Sigma^+(1765)$ production and smaller by about one order of magnitude than the cross section for $K^{\pm}(890)$ production by Σ^- observed in our experiment [23, 24]. The $x_{\rm F}$-spectrum of the f_2' is softer ($n = 4 \pm 1$) than that of Σ^* production by Σ^- ($n \approx 1$) and about the same as that of $K^{\pm}(890)$ production by Σ^- ($n = 3 - 5$).

The value of the coefficient α describing the A-dependence of the cross section, $\alpha = 0.68 \pm 0.05$ corresponds to the value 2/3 expected for coherent production on nuclei and is in good agreement with the values observed for hyperon and meson production in our experiment.

6.4 Search for $H \to \Lambda\Lambda$

The search for exotic states has been one of the major topics of experiment WA89. Using our large sample of observed $\Lambda\Lambda$ pairs we searched for the exotic H particle, which is believed to be the most likely one to exist because of its high symmetry. The decay channel of the H particle depends on its mass, the $\Lambda\Lambda$ mass (2231 MeV/c^2) being the dividing line between strong and weak decays. Our cross section limit for the production of $H \to \Lambda\Lambda$ by Σ^- is two orders of magnitude below the production of $\Lambda\Lambda$ pairs.

Acknowledgements. It is a pleasure to thank J. Zimmer and G. Konorova for their support in setting up and running the experiment. We are also indebted to the staff of the CERN Omega spectrometer group for their help and support, to the CERN EBS group for their work on the hyperon beam line and to the CERN accelerator group for their continuous efforts to provide good and stable beam conditions.

[2] this code is public and is available from the authors on request

References

1. M.I. Adamovich et al., Eur. Phys. J. C **26**, 357 (2003)
2. M.I. Adamovich et al., Phys. Rev. C **65**, 042 202 (2002)
3. D. Bogert et al., Phys. Rev. D **16**, 2098 (1977)
4. E. Andersen et al., J. Phys. G: Nucl. Part. Phys. **25**, 423 (1999)
5. W. Brückner et al., Nucl. Instrum. Methods A **378**, 451 (1996)
6. Y.A. Alexandrov et al., Nucl. Instrum. Methods A **408**, 359 (1998)
7. W. Beusch, CERN/SPSC/77-70
8. M.I. Adamovich et al., Z. Phys. C **76**, 35 (1997)
9. R.T. Edwards et al., Phys. Rev. D **18**, 76 (1978)
10. M.I. Adamovich et al., Eur. Phys. J. C **22**, 255 (2001)
11. R. Blankenbecler, S.J. Brodsky, Phys. Rev. D **10**, 2973 (1974)
12. The Particle Data Group, J. Phys. G: Nucl. Part. Phys. **33**, 1 (2006)
13. G.J. Feldman, R.D. Cousins, Phys. Rev. D **57**, 3873 (1998)
14. T. Sjöstrand, Comput. Phys. Commun. **82**, 74 (1994)
15. A.B. Kaidalov, K.A. Ter-Martirosyan, Sov. J. Nucl. Phys. **39**, 1545 (1984)
16. A.I. Veselov, O.I. Piskounova, K.A. Ter-Martirosyan, Phys. Lett. B **158**, 175 (1985)
17. A.B. Kaidalov, O.I. Piskounova, Sov. J. Nucl. Phys. **41**, 1278 (1985)
18. A.B. Kaidalov, O.I. Piskounova, Z. Phys. C **30**, 145 (1986)
19. A.B. Kaidalov, Sov. J. Nucl. Phys. **45**, 1450 (1987)
20. S.F. Biagi et al., Z. Phys. C **9**, 305 (1981)
21. S.P. Baranov, hep-ph/0209363 HIPPOPO
22. S.P. Baranov, Lebedev Institute of Physics report **42**, 1 (1998)
23. M.I. Adamovich et al., Eur. Phys. J. C **50**, 535 (2007)
24. M.I. Adamovich et al., Eur. Phys. J. C **22**, 47 (2001)
25. R.L. Jaffe, Phys. Rev. Lett. **38**, 195 (1977)
26. F. Close, An introduction to Quarks and Partons (Academic Press, 1989) 5th printing
27. K.F. Liu et al., Phys. Lett. B **113**, 1 (1982)
28. P.J. Mulders et al., J. Phys. G **9**, 243 (1983)
29. U. Straub et al., Nucl. Phys. A **508**, 385c (1990)
30. S.V. Bashinsky, R.L. Jaffe, Nucl. Phys. A **625**, 167 (1997)